Remote Sensing Reviews, 1994, Vol. 8, pp. 271–311
Photocopying permitted by license only

Printed in the United States of America

Sampling the Surface Bidirectional Reflectance Distribution Function (BRDF): 1. Evaluation of Current and Future Satellite Sensors

M. J. BARNSLEY,* A. H. STRAHLER,** K. P. MORRIS† AND J-P. MULLER‡

*Remote Sensing Unit, Department of Geography, University College London, 26 Bedford Way, London, WC1H OAP, England
**Department of Geography and Center for Remote Sensing, Boston University, 675 Commonwealth Avenue, Boston, MA 02215, USA
†Natural Environment Research Council, Image Analysis Unit, Plymouth Marine Laboratory, Plymouth, England
‡Department of Photogrammetry and Surveying, University College London, Gower Street, London, WC1 6BT, England

ABSTRACT

The Bidirectional Reflectance Distribution Function (BRDF) of earth surface materials contains information relating to their physical structure and composition that cannot be inferred from their spectral properties alone. Knowledge of the BRDF is also critical to the accurate retrieval of earth surface albedo, since the BRDF describes the angular distribution of reflected radiation under given illumination conditions. Although the BRDF cannot be measured directly, it can be *estimated* using models of surface scattering in conjunction with reflectance data acquired at different viewing and illumination angles. The ability of a satellite sensor to characterise the BRDF of any point on the earth's surface is therefore dependent on (i) the range of view angles over which it is able to acquire data, (ii) the orbital characteristics of the satellite on which it is mounted, and (iii) the time period over which the data are recorded. This paper explores the BRDF sampling capabilities of several satellite sensors currently in operation (Landsat TM, SPOT HRV, NOAA AVHRR and ERS-1 ATSR) or proposed for launch in the near future (MISR and MODIS). Sensors that are capable of off-nadir viewing solely by virtue of having a wide field-of-view (e.g. NOAA-AVHRR) or through across-track pointing (e.g. SPOT-HRV) provide a relatively sparse sample of the BRDF. On the other hand, future sensors with along-track pointing, such as the MISR instrument of NASA's Earth Observing System (EOS), will provide a much more complete sample and are therefore better able to characterise the surface BRDF and albedo. Sensors such as these are also better equipped to obtain data at and around the 'hot spot' and, consequently, have the potential to extract detailed information on the biophysical properties of earth surface materials.

INTRODUCTION

Over the last twenty years, there has been a continuing interest in the angular reflectance properties of earth surface materials—that is, how their reflectance varies according to the angle of both the sun and the sensor (Salomonson and Marlatt, 1971; Suits, 1972; Kriebel, 1978; Kimes, 1983; Barnsley, 1984). Recent research in this area has highlighted the close relationship between the 3-D geometry of natural surfaces and their angular reflectance properties. In the case of simple, uniform vegetation canopies, such as cereal crops, the controlling factors are believed to be the inclination and orientation of the plant elements (leaves, stems etc.), together with the density of plant material (Goel and Thompson, 1985; Goel and Grier, 1986; Gerstl and Simmer, 1986; Goel, 1987; Otterman et al., 1987; Ross and Marshak, 1988; Goel and Reynolds, 1989; Barnsley and Kay, 1990; Pinty et al., 1990; Verstraete et al., 1990; Goel et al., 1991). For vegetation cover comprised of discrete canopy elements, such as woodland, factors of individual canopy size, shape and density are important (Li and Strahler, 1986, 1992; Nilson and Peterson, 1991). While for bare soil, surface roughness is thought to play a critical rôle (Otterman, 1985; Cierniewski, 1987, 1989; Deering et al., 1989; Pinty et al., 1989; Jackson et al., 1990).

Vegetation canopies often exhibit a pronounced peak in reflectance in the backscatter direction (i.e. where the sun and the sensor are at the same angular position relative to a given point on the earth surface), known as the 'hot spot' (Suits, 1972) or 'opposition surge' (Hapke, 1986). The amplitude and the angular width of this feature are thought to be closely related to specific biophysical parameters, such as average leaf size, leaf-area index and leaf-inclination angle, as well as crown size, shape and density (Gerstl and Simmer, 1986; Li and Strahler, 1986, 1992; Ross and Marshak, 1989; Brakke and Otterman, 1990; Pinty et al., 1989; Strahler and Jupp, 1990; Jupp and Strahler, 1991). The implication of these studies is that, all other things being equal, it may be possible to extract detailed information about a surface, over and above that available from multispectral and multitemporal analyses, through knowledge of its angular reflectance properties.

Interest in the angular reflectance properties of earth surface materials also stems from the need to estimate their albedo, a parameter of great importance in global climate modelling (Dorman and Sellers, 1989). Albedo is commonly defined as the reflectance of a surface integrated with respect to both wavelength (usually between 0.3 μm and 3.0 μm) and angle (i.e. for all directions within the hemisphere above the surface). In practice, however, albedo is usually estimated from measurements of spectral reflectance obtained close to nadir (Pinker, 1985; Pinty and Raymond, 1987; Saunders, 1990). The implicit assumption is either that earth surface materials exhibit Lambertian (isotropic) reflectance properties or that the reflectance measured in the nadir-viewing position closely approximates that averaged over the entire hemisphere above the target. For most natural surfaces, neither of these conditions is necessarily true and, as a result, estimates of albedo derived in this way have been shown to be in error by as much as 45% (Kimes and Sellers, 1985; Kimes et al., 1987).

More accurate and reliable estimates of earth surface albedo can only be obtained through knowledge of the Bidirectional Reflectance Distribution Function (BRDF). The BRDF is an intrinsic property of a surface, which describes the angular distribution of radiation reflected by it, for all angles of exitance and under any given illumination geometry (Nicodemus et al., 1977). Integration of the BRDF with respect to both wavelength and the angle of exitance yields the albedo.

If the BRDF of a surface could be measured completely and without error it would be possible to determine the albedo of that surface *precisely*. Similarly, with the aid of an appropriate physical model of surface scattering, it would also be possible to derive values for certain parameters describing the 3-D geometry of the target (Barnsley and Muller, 1991; Pinty and Verstraete, 1991). Unfortunately, the BRDF cannot be measured directly. This is because it is a ratio of infinitesimal elements of solid angle and wavelength, and as such does not include measurable quantities of radiant flux (Nicodemus et al., 1977). Furthermore, it is neither practical nor possible to record reflectance data for all angles of incidence and exitance. Instead, the BRDF—and, consequently, other parameters derived from it—must be *estimated* from a limited number of angular reflectance measurements made over finite intervals of solid angle and wavelength, using sensors capable of viewing a target at a variety of different angles.

In this context, it is instructive to think of an individual measurement of angular reflectance (i.e. one obtained under a given viewing and illumination geometry) as a *sample* value drawn from the *population* of all such values (i.e. the BRDF). Clearly, then, the accuracy with which the BRDF and related parameters can be estimated will be dependent on both the size of the sample and its angular distribution within the viewing and illumination hemispheres. For spaceborne sensors, these will be conditioned both by the design and operation of the sensing instrument and by the characteristics of the orbit into which it is placed. Tables 1 and 2 summarise the salient design features of some current and planned spaceborne imaging sensors and their orbits. In the remainder of this paper, we examine the ability of these sensors to sample the BRDF of earth surface materials and consider the implications of their angular sampling capabilities for the accurate determination of the BRDF, albedo and other surface biophysical parameters.

SAMPLING THE SURFACE BRDF—CONSIDERATIONS RELATING TO SENSOR GEOMETRY AND SATELLITE ORBITAL CHARACTERISTICS

Current Satellite Sensors

Sensor Viewing Geometry

Arguably, the most important factor controlling a sensor's ability to sample the surface BRDF is its capacity to record data at several different view angles. Currently, most spaceborne, earth-imaging sensors have a fixed viewing geometry,

TABLE 1
Nominal Characteristics of Various Current Satellite Sensors Capable of Off-Nadir Viewing

Sensor	TM	HRV	AHVRR (pm)	AVHRR (am)	ATSR
Type	Whiskbroom scanner	Pushbroom scanner	Whiskbroom scanner	Whiskbroom scanner	Scanning Radiometer
Across-track FOV or Scan Angle	15°	8.26°	110°	110°	102°
Along-track FOV	n/a	n/a	n/a	n/a	n/a
Pointing Angle, Across-track	n/a	±27°	n/a	n/a	n/a
Pointing Angle, Along-track	n/a	n/a	n/a	n/a	46.9° and nadir.
Spectral Bands	7	3 + 1	5	5	3 (+1)
Spectral Range (μm)	0.45 - 12.5	0.50 - 0.89	0.58 - 12.5	0.58 - 12.5	1.6/3.7 - 12.0
Spatial Resolution (Nadir)	30m (Vis/IR) 120m (TIR)	10m (Pan) 20m (XS)	1.1km	1.1km	1km
Platform	Landsat 5	SPOT-2	NOAA-9	NOAA-10	ERS-1
Launch Date	March 1984	January 1990	December 1984	1986	1991
Orbital Elevation	705km	832km	857km	852km	797km
Equatorial Crossing Time and Direction	09.45 ± 15 min Ascending	10.30 ± 15 min Ascending	02.30 Descending 14.30 Ascending	07.30 Descending 19.30 Ascending	10.30 Descending
Orbital Inclination Angle	98.2°	98.7°	98.8°	98.8°	96.8°
Repeat Cycle	16 days	26 days	n/a	n/a	35 days
Orbital Period (Seconds)	5934	6106	6120	6120	6055
No. of Orbits in Cycle	233	369	n/a	n/a	???
Days for Global Coverage (Nadir viewing mode)	16	26	2	2	? days

centered on nadir. With a design such as this, only one measurement (albeit multispectral) can be made of a given point on the earth surface per overpass. The view angle on each occasion is determined by the distance between the point viewed and the sub-satellite point, together with the altitude of the satellite. For instruments such as the Landsat Thematic Mapper (TM), the scan angle (11°) is such that all measurements will be obtained close to nadir and thus the opportunity to explore the surface BRDF is very limited. Nevertheless, angular variations in reflectance are still present in data acquired by this sensor. The field-of-view of the SPOT-HRV (Haut Resolution Visible) instruments is even narrower (8.26°), but their capability to point up to ±27° off-nadir, perpendicular to the orbital ground-track, allows a greater range of viewing geometries to be sampled. Taking into account the effect of earth surface curvature, view zenith angles of up

TABLE 2
Nominal Characteristics of Various Future Satellite Sensors capable of Off-Nadir Viewing
(N.B. tbd = to be determined)

Name	POLDER	ASTER	MODIS-N (AM)	MODIS-N (PM)	MISR
Type	Framing CCD Array	Multispectral Imager	Multispectral imager	Multispectral imager	Pushbroom scanner
Across-track FOV or Scan Angle	84°	6.09° (VNIR - nadir) 5.19° (VNIR - forward) 4.90° (SWIR and TIR)	110°	110°	28°
Along-track FOV	102°	n/a	n/a	n/a	n/a
Pointing Angle, Across-track	n/a	8.55°	n/a	n/a	n/a
Pointing Angle, Along-Track	n/a	-27.6° and 0° (VNIR only)	n/a	n/a	+58.0°, +51.2°, +40.0°, +23.3°, 0.0°, -23.3°, -40.0°, -51.2°, -58.0°
Spectral Bands	8	14	36	36	4
Spectral Range (μm)	0.443 - 0.91	0.50 - 11.65	0.40 - 14.5	0.40 - 14.5	0.40 - 0.86
Spatial Resolution (Nadir)	6km x 7km	15m (VNIR), 30m (SWIR) and 90m (TIR)	250m, 500m, 1km	250m, 500m, 1km	240m (local mode), 960m (land), 1.92km (ocean)
Platform	ADEOS	EOS (pm)	EOS-AM	EOS-PM	EOS-AM
Launch Date	1996	1998	1998	1998	1998
Orbital Elevation	c.800km	705km	705km	705km	705km
Equatorial Crossing Time and Direction	tbd	13.30 Ascending	10.30 Descending	13.30 Ascending	10.30 Descending
Orbital Inclination Angle	tbd	98.25°	98.25°	98.25°	98.25°
Repeat Cycle	tbd	16 days	16 days	16 days	16 days
Orbital Period (Seconds)	tbd	5934	5934	5934	5934
No. of Orbits in Cycle	tbd	233	233	233	233
Days for Global Coverage (Nadir viewing mode)	tbd	16	1	1	9

to 35.8° may be sampled at the extreme edges of the fully-pointed scan (Figure 1). Finally, the 110° swath of NOAA's AVHRR (Advanced Very High Resolution Radiometer) sensors offers still greater possibilities for sampling the BRDF, allowing a view zenith angle of almost 70° at the extreme edge of any scan line.

A fourth sensor that can be used to acquire data at different view angles is the Along-Track Scanning Radiometer-1 (ATSR-1) on board ERS-1 (Prata

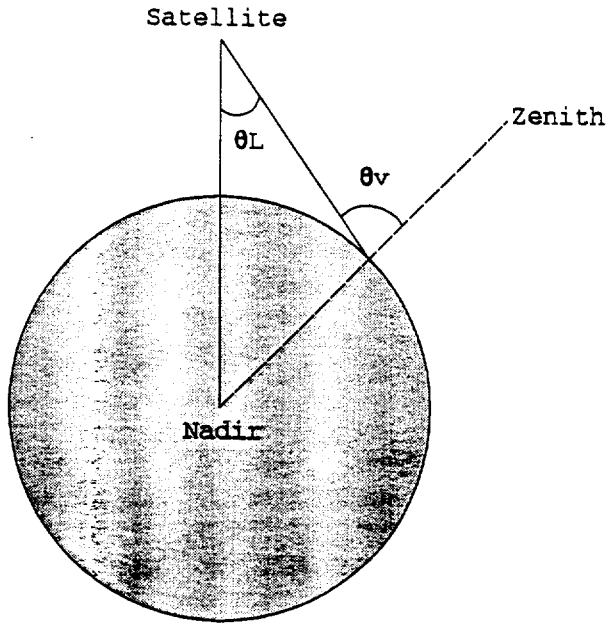

FIGURE 1 Relationship between sensor look angle (θ_l) and view zenith angle (θ_r), taking into account the effect of earth surface curvature.

et al., 1990). This instrument has an unusual conical scanning pattern which permits two separate views of a 256-km-wide swath within a single orbit. Data are recorded almost simultaneously along two scan lines which describe arcs across the earth surface. The axis of the conical scan lies at 23.45° forward from nadir in the along-track direction. As a result, the first arc is centered on the sub-satellite (i.e. nadir) point, while the second is pointed forward of the satellite at 46.9° along-track (equivalent to a 55° view zenith angle). Consequently, any point on the ground falling within the nadir swath will be imaged twice during a single overpass. The current version of this instrument is a 3-channel radiometer operating in the thermal infrared (centered on 3.7 μm, 11.0 μm and 12.0 μm), although one of the channels (3.7 μm) can be switched to operate in the shortwave infrared (1.6 μm) during the daytime (descending) overpass. A second version, ATSR-2, scheduled for launch on ERS-2 in 1994, will have three further channels in the visible and near-infrared (centered on 0.555 μm, 0.659 μm and 0.865 μm).

Satellite Orbital Characteristics

The ability to sample the surface BRDF is influenced not only by the viewing geometry of the sensor, but also by the orbital characteristics of the satellite platform on which it is mounted and the latitude of the ground point being observed. For instance, the orbital repeat cycle of Landsat-4 and 5 is designed, in conjunction with the characteristics of its sensors, to cover the earth fully in a 16-day cycle. However, since the orbits converge towards the poles, high latitude sites may be viewed on more than one occasion in the 16-day sequence. This allows data to be collected from several, slightly different viewing positions. Similarly, the across-track pointing capability of the SPOT-HRV sensors increases the poten-

tial number of samples of the BRDF that they can acquire. As many as 5 viewing positions are possible at the equator during a single orbital repeat cycle (26 days), increasing to 12 at 50° latitude, and more beyond. Finally, NOAA-AVHRR's very wide field-of-view extends global coverage to once every other day, permitting a maximum of 27 looks over 16 days for a point at the equator and more than 40 looks at latitudes greater than 50°. Figure 2 demonstrates the angular sampling characteristics of Landsat TM, SPOT-HRV and NOAA-AVHRR over a 16-day period around the March equinox, for a point located at latitude 50°N.

Since the orbital sensors of interest here record reflected solar radiation, the illumination geometry must also be considered. The solar illumination angle is dependent on the time of day, the time of year and the latitude of the ground location. Even where a sensor is mounted on a satellite in sun-synchronous orbit, the solar zenith and solar azimuth angles will vary appreciably throughout the year for a fixed point of observation on the ground. They will also vary when the point is viewed from different orbits in the repeat cycle. This is due to the difference in longitude and, hence, in the local solar time between the sub-satellite point and the area being observed. The same effect means that for wide scan-angle sensors, such as AVHRR, the illumination geometry varies across a single scan line, even though the data are collected almost instantaneously.

The extent to which angular reflectance measurements collected at different times and/or on different days can be regarded as samples of the same BRDF depends on the nature of the ground surface, as well as variations in atmospheric conditions. Most land surfaces will change significantly throughout the year, as they respond to the natural cycles of the biosphere and hydrosphere. Even over the period of a few hours, ground characteristics may change markedly as, for example, in the wetting and drying of soil during and after rainfall. Moreover, atmospheric parameters may also be expected to vary from day-to-day. Therefore, given the current generation of spaceborne imaging sensors, the optimum strategy for sampling surface BRDFs must be to balance the number and angular distribution of reflectance measurements with the length of time over which they are acquired.

Future Satellite Sensors

It is possible to design sensors that can make measurements of reflectance at a number of different view angles relative to a fixed point on the ground during a single overpass. This ensures that the ground BRDF and atmospheric properties remain reasonably stable during the period of observation. Three approaches are possible. The first is to design an instrument with a two-dimensional CCD array and a wide field-of-view in both the along-track and the across-track directions. A sensor such as this can be operated in a manner analogous to an aerial survey camera, recording a sequence of overlapping, digital images as the platform passes over the study area. A fixed point on the ground may therefore be sensed at different view angles within each image. The second approach is to equip an instrument with multiple fore-, aft- and nadir-looking sensors so that a sequence of images obtained at different view angles can be acquired within a very short

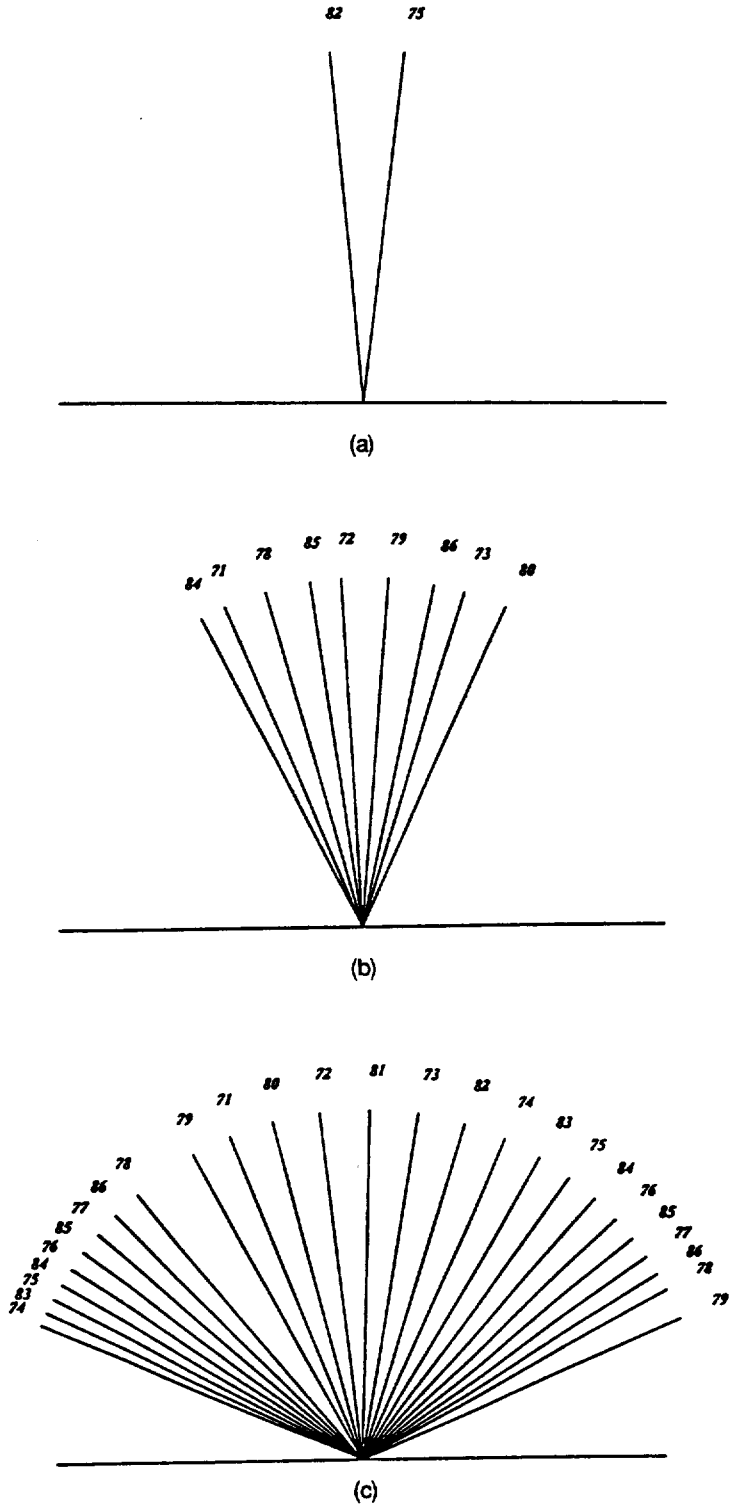

FIGURE 2 Angular sampling capabilities of three current satellite sensors over a 16-day period around the March equinox for a target located at 50° N. (a) Landsat TM; (b) SPOT HRV; (c) NOAA-10 AVHRR (7:30am overpass only). Numbers indicate Julian dates on which the target is imaged by the sensor. Lines indicate the sensor view angle (θ_r) at which the target is sensed on each occasion.

period of time. The third approach is to make the instrument pointable in the along-track direction, thereby allowing repeated imaging of the ground point as the orbital platform approaches the target, overflies it and recedes from it.

The first approach outlined above is to be adopted by the French sensor POLDER (Polarisation and Directionality of the Earth's Reflectance), which is scheduled for launch on board ADEOS (Advanced Earth Observation Satellite) in 1996 (Deschamps et al., 1990; Deuzé et al., 1991). POLDER will consist of a 242 by 548 element CCD array[1] defining a rectangular field-of-view of approximately 86° (along-track) by 102° (across-track). Multispectral and multi-polarisation data will be acquired using a rotating filter wheel which will accommodate 16 filters, including a dark current measurement. More specifically, data will be obtained in six non-polarised spectral wavebands centered at 0.443 μm, 0.49 μm, 0.565 μm, 0.765 μm, 0.763 μm and 0.91 μm, as well as in three different polarisations using wavebands centered on 0.443 μm, 0.665 μm and 0.865 μm. The bandwidth will be 20 nm, except in the case of the 0.765 μm and 0.763 μm channels which will have bandwidths of 40 nm and 10 nm, respectively. POLDER will provide data at a spatial resolution of 6 km × 7 km.

Two instruments scheduled for launch in 1998 as part of NASA's Earth Observing System (EOS) will make use of multiple fore-, aft- and nadir-looking sensors to acquire angular reflectance data. These instruments are known as MISR (Multi-angle Imaging Spectro-Radiometer) and ASTER (Advanced Spaceborne Thermal Emission and Reflection Radiometer) (Diner, 1988; Diner et al., 1989; NASA, 1990). MISR will utilise nine CCD-array cameras to collect images simultaneously at four off-nadir angles between 23.3° (view zenith angle = 26.1°) and 58.0° (view zenith angle = 70.5°) in both the fore and aft directions, as well as at nadir. Each camera will record data in four narrow spectral bands in the range 0.4 μm–0.9 μm. By selection of appropriate focal lengths for each camera, MISR's spatial resolution is independent of sensor look angle in the along-track direction. The six outermost cameras will normally acquire data at a resolution of 1.92 km over the oceans and 960 m over land, with the three innermost cameras acquiring data at a resolution of 240 m for stereo coverage of clouds and the land surface. A 'local mode' is also possible, in which all nine cameras can report 240 m data for a 360 km by 300 km target, though with a concomitant increase in the data rate.

By contrast, ASTER is an imaging radiometer which will acquire nadir-viewing data in 14 spectral channels between 0.5 μm and 11.65 μm, at a spatial resolution of between 15 m and 90 m depending on the waveband (NASA, 1990). Data for one of the three channels centered in the visible and near-infrared will also be acquired at an angle of 27.6° along-track in the aft direction to provide stereo coverage (Kahle, pers. comm.). ASTER will have a 60 km ground swath which will be pointable up to ±8.55° cross-track to provide complete global coverage.

The third method for collecting measurements of reflectance at different sensor view angles within a single overpass was to be adopted by two other EOS in-

[1]The CCD elements will be binned two-by-two in the long axis to produce images of 242 by 274 pixels in size (Deschamps, pers. comm.).

struments, namely HIRIS (High Resolution Imaging Spectrometer) and MODIS-T (Moderate Resolution Imaging Spectrometer-Tilt) (NASA, 1986a,b; Goetz and Herring, 1989; Salomonson et al., 1989; NASA, 1990; Ardanuy et al., 1991). The design specification for HIRIS incorporated a very narrow field-of-view (2.1°), but with the capability to point the sensor up to 56° and 30° along track in the fore and aft directions, respectively, as well as ±45° in the across-track direction (NASA, 1986a,b; Goetz and Herring, 1989; NASA, 1990). By contrast, MODIS-T was intended to have a fixed scan-angle of ±45° across track, but was to be pointable up to ±50° in the along-track direction (Ardanuy et al., 1991). Both instruments were intended to be imaging spectrometers: HIRIS was to have 192 narrow spectral bands between 0.4 μm and 2.45 μm, while MODIS-T was intended to have 32 bands between 0.4 μm and 0.88 μm. The principal differences between the two sensors were to be their spatial resolving power and areal coverage: HIRIS was to have a high spatial resolution (30 m at nadir) and a 30 km swath, whereas MODIS-T was to have a much coarser spatial resolution (1.1 km at nadir) and a 1800 km swath. Unfortunately, neither of these two sensors now seems likely to fly on the EOS platform, due to budgetary constraints.

Despite the demise of the planned MODIS-T, its sister instrument MODIS-N (Moderate Resolution Imaging Spectrometer-Nadir)[2] seems likely to be launched in 1998 along with MISR and ASTER. In terms of sensor geometry, MODIS-N bears a strong resemblance to the current generation of AVHRR instruments. In particular, MODIS-N will acquire data at a spatial resolution of 1 km over a 1500 km (110°) swath. Unlike AVHRR though, MODIS-N will record data in 36 narrow spectral channels. Although not primarily intended for angular reflectance studies, the rôle of MODIS-N in sampling the BRDF will be discussed in Section 2.

Although all of the instruments discussed so far will be useful for BRDF studies, each has specific characteristics that, in practice, will distinguish its use. Firstly, each sensor differs in terms of spectral range and the number of wavebands recorded—producing images in as few as four bands in the case of MISR, or as many as 16 bands in the case of POLDER. Secondly, their spatial resolutions differ markedly, ranging from 15 m (ASTER) to 7 km (POLDER). Thirdly, their angular resolution capabilities differ—MISR will obtain images at nine different angles per overpass, whereas tiltable sensors (e.g. HIRIS) can, in theory, obtain many more, albeit only for selected areas of the earth surface (this point is discussed further later in this paper). Finally, each instrument will have different operational constraints, depending on the nature of its mission.

SAMPLING THE SURFACE BRDF—USES AND COMPLICATIONS

In planning the acquisition of angular reflectance measurements, it is important to bear in mind the reasons for collecting such data. With respect to studies of the land surface, there are two primary objectives which may require contrasting

[2]Now referred to by NASA simply as MODIS. However, to avoid confusion here these instruments will be referred to as MODIS-N and MODIS-T for the remainder of this paper.

strategies in terms of sampling the BRDF. The first involves data collection at a variety of different zenith and azimuth angles throughout the viewing hemisphere. The second involves obtaining a dense sample of angular reflectance measurements at or close to the hot spot.

The first objective is to provide a "correction" for angular reflectance effects on commonly-used products of earth-resource studies. For example, the Normalised Difference Vegetation Index (NDVI), which is widely used in studies of global biological productivity and efficiency (Goward et al., 1991; Gutman, 1991), is known to be strongly influenced by sensor view angle (Holben and Fraser, 1984; Paltridge and Mitchell, 1990). Accordingly, scientists of the MODIS land team are planning to correct the NDVI product derived from MODIS-N data, through knowledge of the surface BRDF inferred from other EOS instruments (Running et al., 1993). For this purpose, the emphasis is simply placed on specifying the BRDF, rather than explaining it. Thus, all that may be needed here is a reasonably accurate empirical representation of the BRDF (Roujean et al., 1990). In these circumstances, it may be preferable to obtain a set of reflectance measurements distributed reasonably evenly throughout the viewing hemisphere. This angular sampling strategy would also be appropriate for studies designed to estimate the hemispherical reflectance (albedo) of surface materials.

The second objective is to infer the values of basic physical parameters that describe the condition of earth surface materials, using knowledge of their BRDFs. Examples include the single-scattering albedo and phase function of surface materials (Hapke, 1981, 1984, 1986; Hapke and Wells, 1984; Pinty et al., 1989); the roughness length of soils and regolith (Hapke, 1984; Cierniewski, 1987, 1989; Pinty et al., 1989); the leaf density, leaf size and average leaf-inclination angle of vegetation canopies (Pinty et al., 1990; Verstraete et al., 1990; Pinty and Verstraete, 1991); and, the crown size, shape and count density for tree stands (Strahler and Jupp, 1990; Jupp and Strahler, 1991). Inferences of this nature cannot be readily achieved by fitting an empirical function to the BRDF. Rather, it requires an appropriate physical model of surface reflectance and inversion of that model to yield the driving parameters (Strahler and Jupp, 1990; Barnsley and Muller, 1991; Pinty and Verstraete, 1991).

Measurements and models of the BRDF of land surface materials have shown that it is most highly structured close to the 'hot spot.' In particular, the shape of the hot spot—in terms of its amplitude and its angular dispersion in both the zenith and azimuth directions—is known to be sensitive to the size, shape, spacing and arrangement of the scattering elements, e.g. soil clods, leaves, tree crowns and terrain facets (Suits, 1972; Gerstl and Simmer, 1986; Li and Strahler, 1986, 1992). Therefore, the viewing strategy that is most likely to be useful for inference of these surface parameters will be one involving a dense angular sample of data collected close to the hot spot.

In a satellite-imaging scenario, collecting data at the hot spot amounts to imaging the shadow[3] of the platform as it moves in orbit. For example, the planned

[3]Obviously, the 'shadow' of the platform is never cast upon the earth due to penumbral effects; it is used here as a device for explaining sensing scenarios.

orbit of the EOS-PM platform, which has an equatorial crossing time of 1:30 pm (daytime ascending node), provides a platform-shadow to the right of the orbital track[4] As the platform rises up from the South Pole to the latitude of the sub-solar point, the shadow will fall behind the spacecraft. For this portion of the orbit, a sensor seeking measurements close to the hot spot will have to image backward and to the right of the platform. When the orbit is closest to the sub-solar point, the shadow of the platform will fall directly to its right and will lie in the imaging plane of a nadir-pointing scanner. Here, the hot spot may be seen by such an instrument if its field-of-view is sufficiently wide. As the satellite passes this position, the shadow will fall in front of the platform and thus near-hot-spot measurements will have to be made to the right and in a forward direction.

Another important reason for examining angular reflectance effects is to determine atmospheric optical conditions for radiometric correction purposes. Thus, by viewing the same area on the ground via different atmospheric path lengths within a short period of time, it may be possible to infer information on the aerosol optical properties of the atmosphere (Diner and Martonchik, 1985; Ioltukhovski, 1991; Martonchik and Diner, 1992). Although the purpose of this paper is not to examine the atmospheric correction problem, it is clearly a most important topic, since the angular reflectance effects of the atmosphere will be superimposed on those of the earth surface (Tanré et al., 1983; Powers and Gerstl, 1988). In all probability, recovery of information about surface characteristics and atmospheric parameters will eventually require simultaneous solution of the radiative transfer through both media, in a coupled model of the ground and the atmosphere (Gerstl and Zardecki, 1985; Liang and Strahler, 1993).

The plan for the remainder of the paper is to review several current and future satellite sensors in the context of the foregoing discussion. Emphasis will be placed on the geometric characteristics of their off-nadir viewing capabilities and salient aspects of the orbital mechanics of the satellites on which they are, or will be, mounted. The BRDF sampling capabilities of each sensor will also be discussed in the context of the requirements for global monitoring of surface biophysical parameters.

EVALUATING THE BRDF SAMPLING CAPABILITIES OF CURRENT AND FUTURE SENSORS

Evaluating the ability of a particular instrument to make useful angular reflectance measurements is a fairly complex task, since it involves not only the characteristics of the instrument itself, but also the orbital parameters of the satellite platform on which it is mounted, the time of year at which the data are collected and the latitude of the ground location. One way to start is to look at the viewing capabilities of each instrument. Nominal specifications for most sensors are usually quoted in terms of angles with respect to the satellite platform. These differ from the actual view zenith and view azimuth angles at the ground, due to

[4]All directions are given with reference to the position of an observer on the platform, facing forward, feet toward the earth.

the curvature of the earth surface (Figure 1) and its rotation under the orbital path of the satellite. Figures 3 to 5 provide polar plots of the maximum viewing 'envelope' of five imaging sensors, expressed in terms of their view zenith and view azimuth angles, calculated using standard spherical trigonometry for satellite platforms located at latitude 50°N, the equator and latitude 25°S, respectively.[5] In these figures, the view zenith angle is plotted radially outwards from the centre (nadir); thus, the concentric circles on the polar grid represent 10° increments of view zenith angle. The view azimuth angles (relative to true north) are represented in terms of angle around the plot. The figures clearly demonstrate the ability of pointable instruments, such as HIRIS, to image freely within most of the viewing hemisphere. It should be noted that the distortion in the viewing envelope encountered at high latitudes is a result of the convergence of the lines of longitude towards the poles.

Although it is helpful to establish the range of view angles over which each sensor can acquire data, a more instructive comparison is to evaluate the ability of each instrument to image a fixed point on the earth surface over a specified period of time. In evaluating this and other scenarios, we use the capabilities of the X-SATVIEW program, developed in the Remote Sensing Unit at University College London.[6] X-SATVIEW determines the number of occasions on which a fixed point on the ground is visible to a sensor in a known orbit, within a specified period of time. This is calculated on the basis of the maximum viewing 'envelope' of the chosen sensor and the nominal orbital characteristics of the satellite on which it is mounted (including its altitude, orbital inclination and orbital period). The view zenith and view azimuth angle at which the ground point is sensed on each such occasion is determined by standard spherical trigonometry, using the GRS-80 spheroid to model the shape of the earth. The solar zenith and solar azimuth angles are calculated in a similar manner, using information on the solar declination angle (a function of the time of year) and the approximate times of imaging (based on the nominal equatorial crossing time of the satellite and its orbital period).

It is important to note from this that X-SATVIEW is intended as a simulation tool. The program does not, for instance, determine the *precise* viewing and illumination geometry for a given location on the ground, using a *specific* satellite sensor, at a given point in time. This requires much more detailed information on the satellite ephemeris which, in any case, is not available for satellite sensors that are yet to be launched. Instead, the aim of X-SATVIEW is to provide a means of simulating the BRDF sampling capabilities that can be achieved using certain combinations of sensor geometry and satellite orbit.

For example, it is possible to consider the range of angular reflectance measurements that could be obtained by a sensor such as the AVHRR mounted on

---

[5]Although they have recently been de-selected from the EOS programme, HIRIS and MODIS-T are included here to illustrate the maximum viewing 'envelope' that can be achieved using sensors which are pointable in the along-track direction.

[6]A copy of the executable code of this program is available for Sun 4 workstations from the principal author.

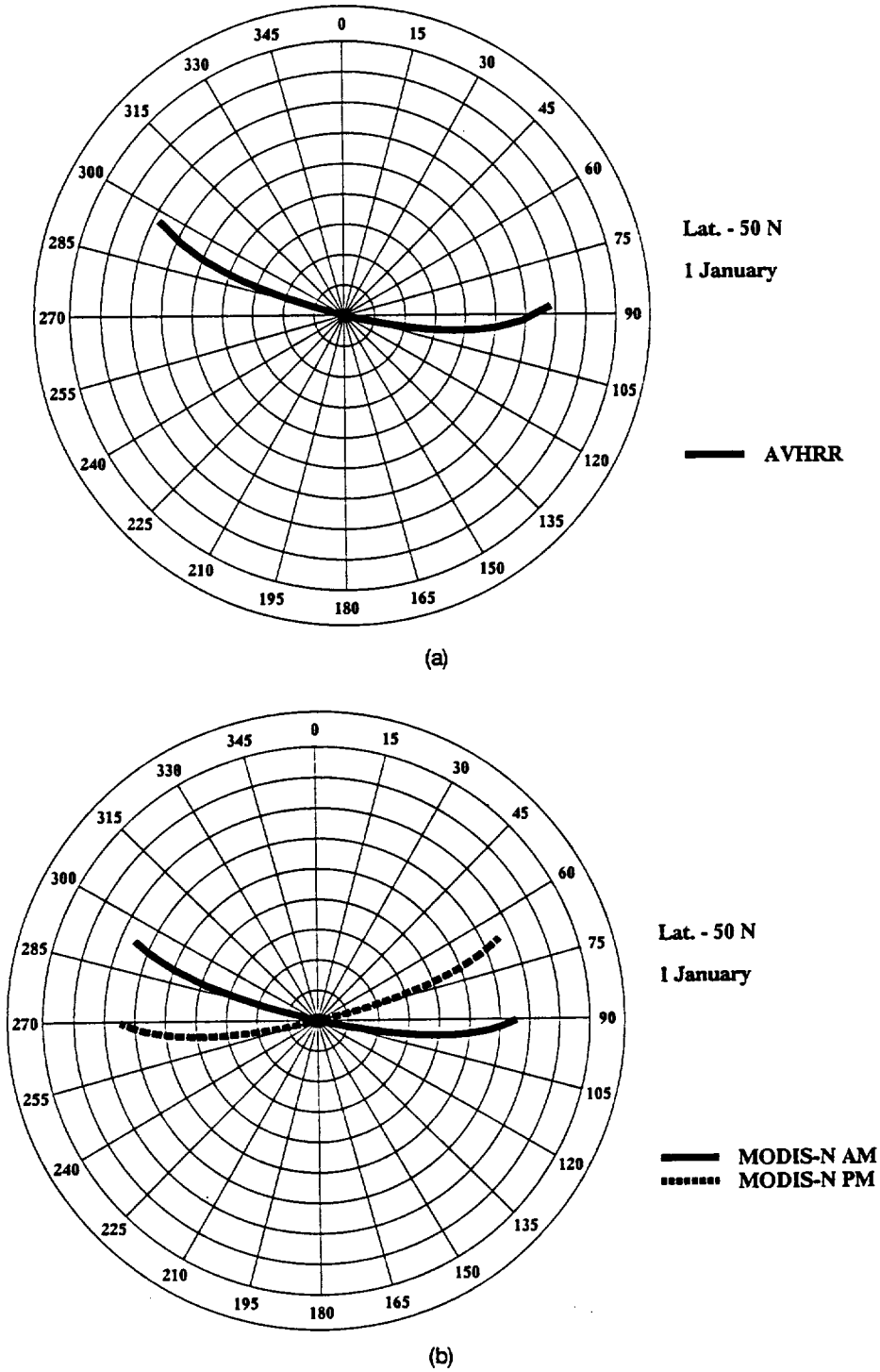

FIGURE 3 Maximum viewing 'envelope' for five satellite sensors located above latitude 50°N. (a) NOAA-9 AVHRR; (b) EOS-AM and EOS-PM MODIS-N; (c) EOS-AM MISR; (d) HIRIS and MODIS-T. Concentric rings denote 10° increments of view zenith angle (θ_r), ranging from 0° (i.e. nadir) at the center of the plot to 90° at the edge. Radial lines denote 15° increments of view azimuth angle (ϕ_r), where 0° = north and 180° = south. N.B. The width of the 'envelope' lines has been exaggerated for diagrammatic purposes.

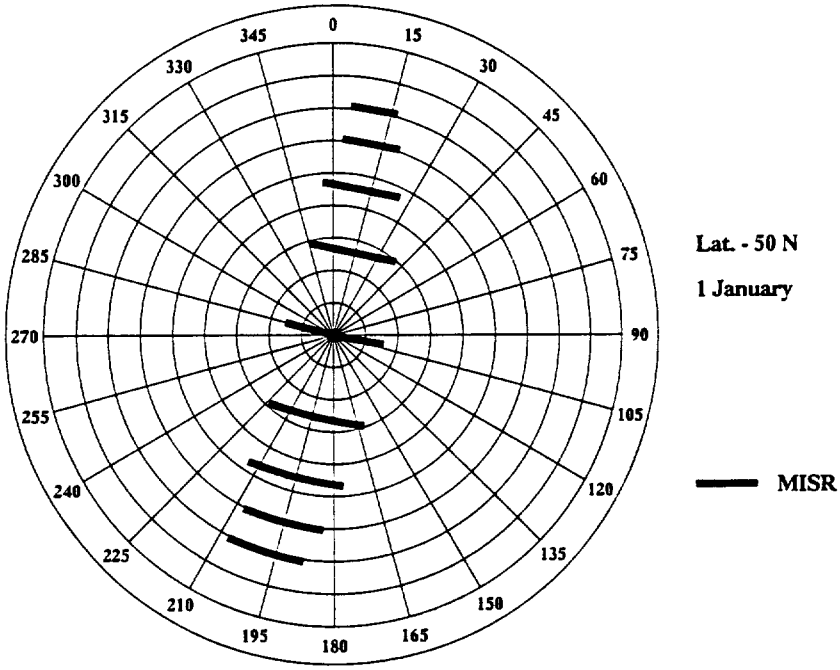

(c)

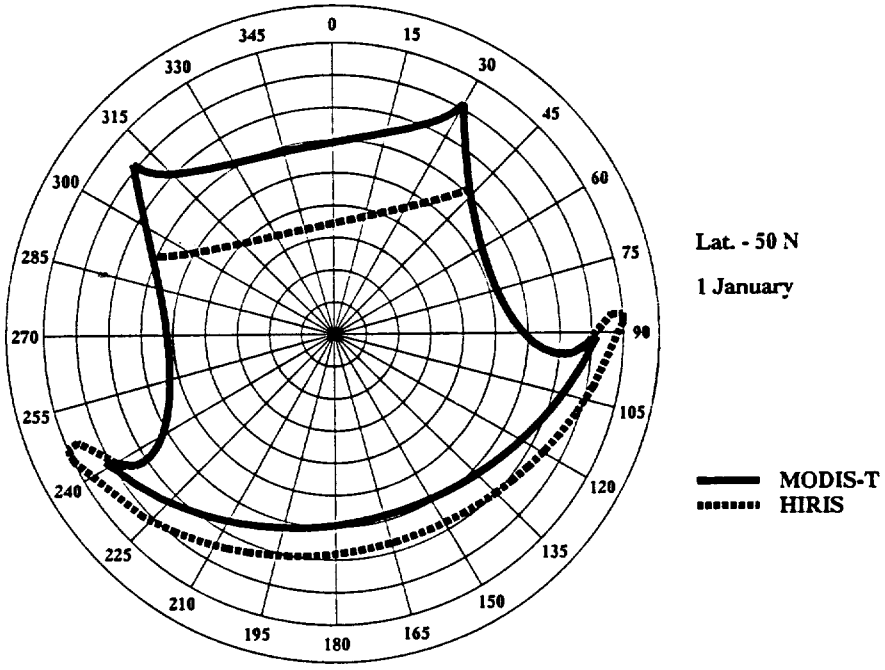

(d)

FIGURE 3 (*Continued*).

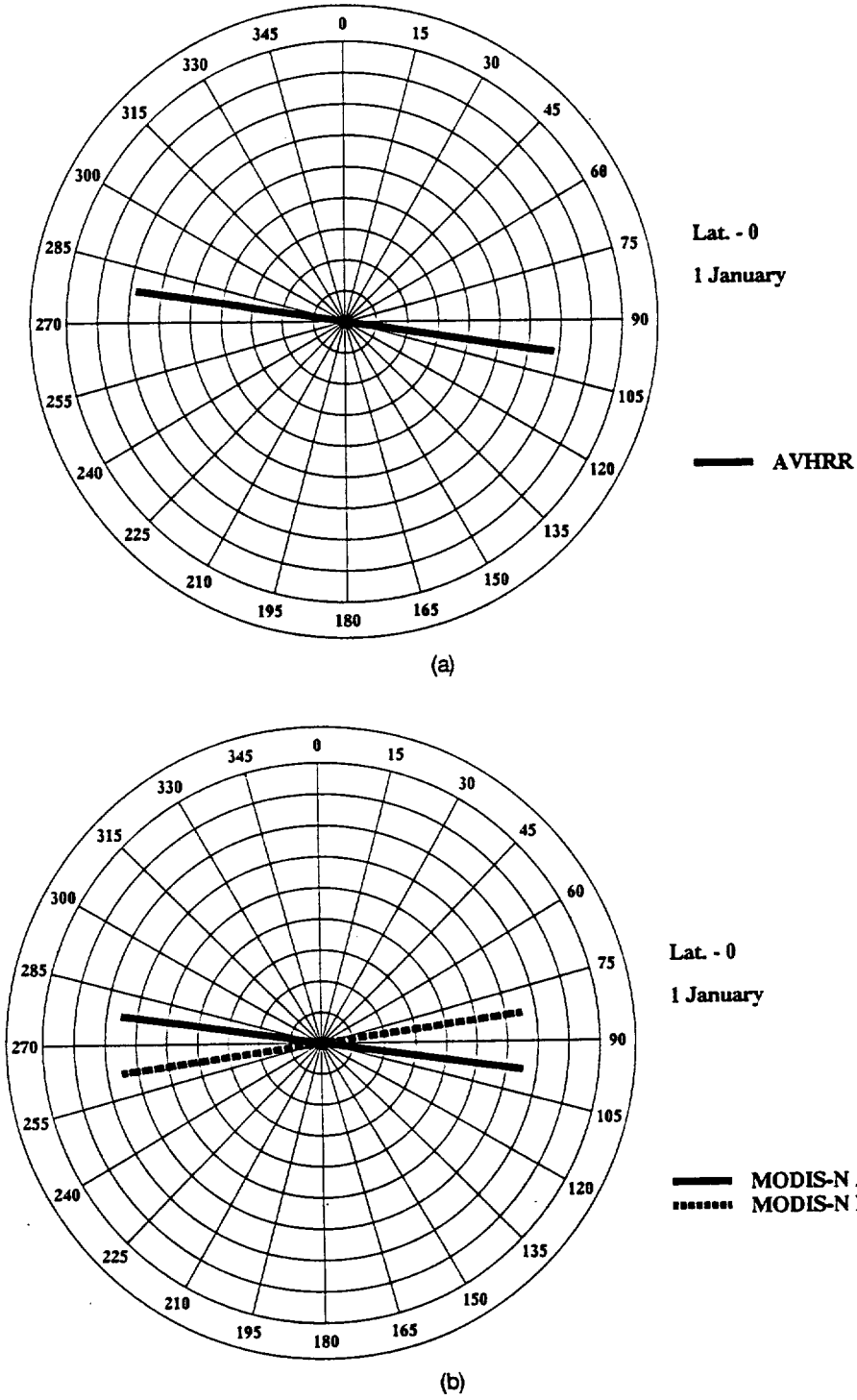

FIGURE 4 Maximum viewing 'envelope' for four satellite sensors located above the equator. (a) NOAA-9 AVHRR; (b) EOS-AM and EOS-PM MODIS-N; (c) EOS-AM MISR; (d) HIRIS and MODIS-T. Concentric rings denote 10° increments of view zenith angle (θ_r), ranging from 0° (i.e. nadir) at the center of the plot to 90° at the edge. Radial lines denote 15° increments of view azimuth angle (ϕ_r), where 0° = north and 180° = south. N.B. The width of the 'envelope' lines has been exaggerated for diagrammatic purposes.

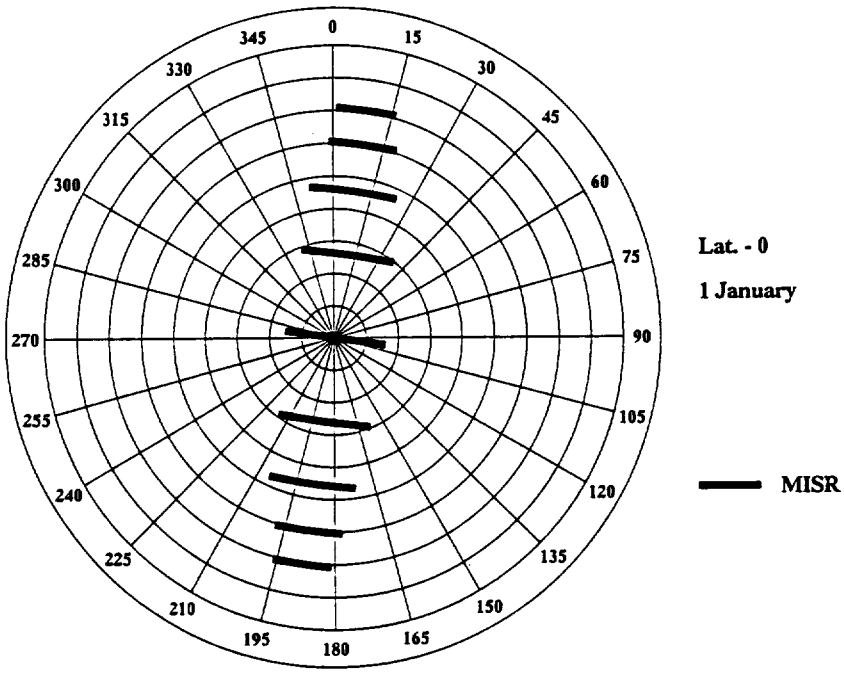

(c)

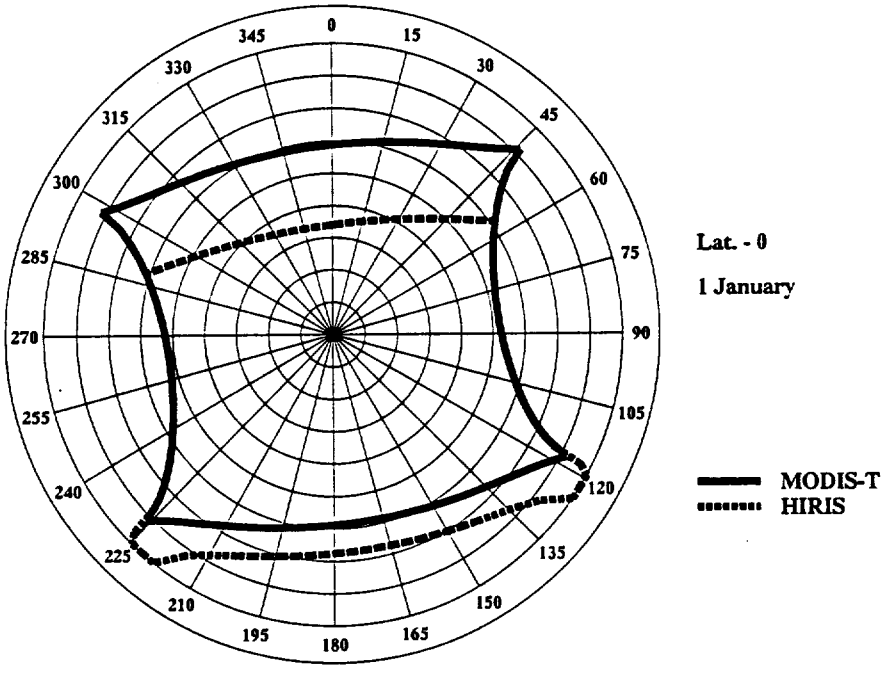

(d)

FIGURE 4 (*Continued*).

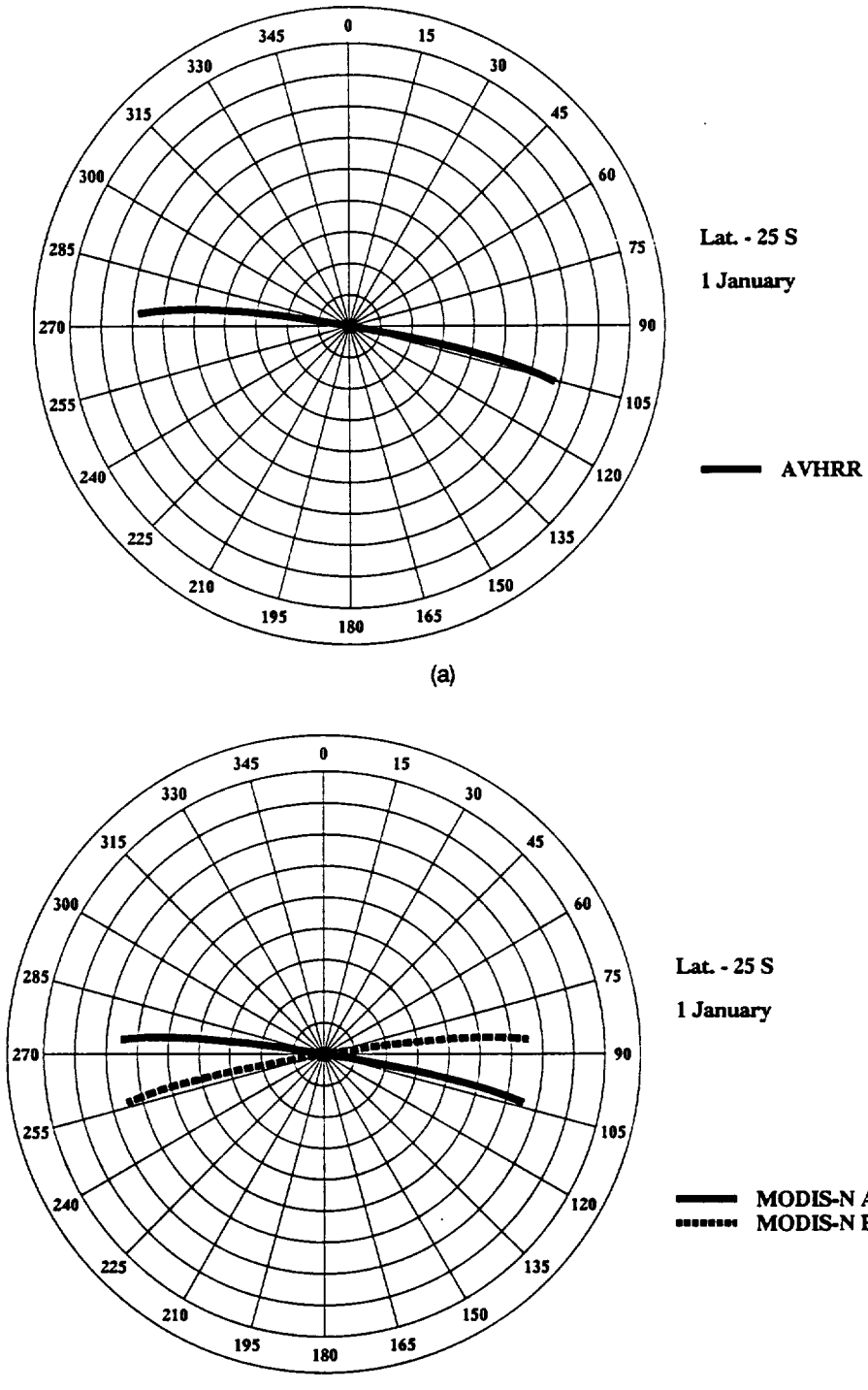

FIGURE 5 Maximum viewing 'envelope' for four satellite sensors located above latitude 25°S. (a) NOAA-9 AVHRR; (b) EOS-AM and EOS-PM MODIS-N; (c) EOS-AM MISR; (d) HIRIS and MODIS-T. Concentric rings denote 10° increments of view zenith angle (θ_r), ranging from 0° (i.e. nadir) at the center of the plot to 90° at the edge. Radial lines denote 15° increments of view azimuth angle (ϕ_r), where 0° = north and 180° = south. N.B. The width of the 'envelope' lines has been exaggerated for diagrammatic purposes.

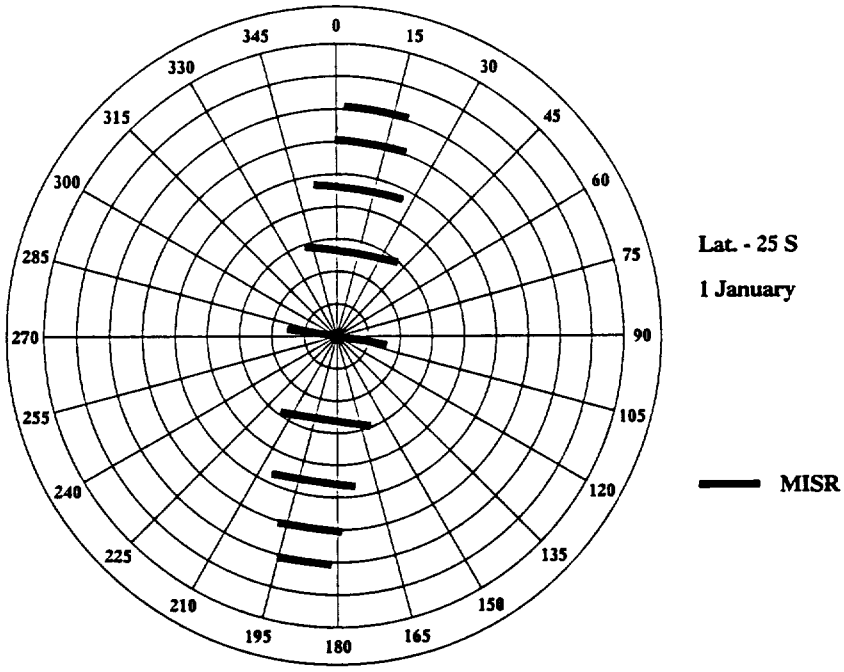

(c)

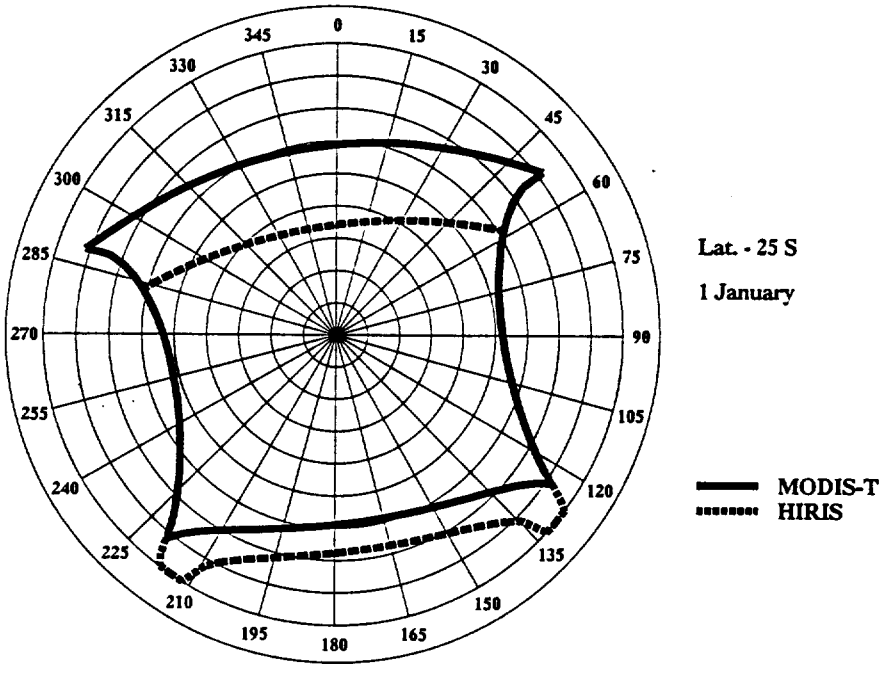

(d)

FIGURE 5 (*Continued*).

TABLE 3
Viewing and Illumination Geometry for Images Acquired for a Ground Point at 50°N by NOAA-9 AVHRR Over a 16-day Period Around the March Equinox

Julian Day	Local Solar Time (h, m, s).	View Zenith Angle (°)	View Azimuth Angle (°)	Solar Zenith Angle (°)	Solar Azimuth Angle (°)	Relative Azimuth Angle (°)
71	13 24 00	60.3	91.5	57.1	205.2	66.3
71	15 06 00	42.4	291.3	67.3	231.7	239.6
72	13 12 00	65.7	89.2	55.9	201.9	67.3
72	14 54 00	31.5	288.9	65.4	229.0	239.8
73	14 42 00	18.0	286.5	63.7	226.3	240.2
74	14 30 00	2.5	284.6	61.9	223.5	241.1
75	14 18 00	13.4	101.7	60.3	220.7	61.1
76	14 06 00	27.9	99.5	58.7	217.7	61.8
76	15 48 00	65.5	299.9	71.2	242.3	237.7
77	13 54 00	39.9	97.2	57.2	214.6	62.6
77	15 36 00	60.6	297.4	69.2	239.9	237.5
78	13 42 00	49.5	94.9	55.8	211.4	63.5
78	15 24 00	54.5	294.9	67.2	237.4	237.5
79	13 30 00	57.1	92.6	54.4	208.1	64.6
79	15 12 00	46.9	292.5	65.3	234.9	237.6
80	13 18 00	63.1	90.3	53.2	204.6	65.7
80	15 00 00	37.2	290.1	63.4	232.3	237.8
81	13 06 00	68.1	88.0	52.1	201.1	66.9
81	14 48 00	25.0	287.7	61.6	229.6	238.1
82	14 36 00	10.4	285.4	59.6	226.8	238.7
83	14 24 00	5.5	102.7	58.0	223.9	58.9
84	14 12 00	20.9	100.6	56.4	220.8	59.8
84	15 54 00	67.6	301.2	69.5	245.5	235.7
85	14 00 00	34.2	98.3	54.8	217.7	60.6
85	15 42 00	63.2	298.7	67.4	243.2	235.5
86	13 48 00	45.0	96.1	53.3	214.5	61.6
86	15 30 00	57.7	296.1	65.4	240.7	235.4

board a satellite with the nominal orbital characteristics of NOAA-9.[7] Table 3 presents the results of this simulation for a ground point at latitude 50°N, during a 16-day period around the March equinox (Julian days 71–86). The table lists the Julian day, local solar time and both the viewing and solar geometry for the 27 possible looks at the target during this time period. On 11 of the 16 days, two looks are possible. View zenith angles range from 3° to 68°, while view azimuth

[7]To avoid these complex semantics, we will refer to this as a simulation of NOAA-9 AVHRR. Simulations for other sensor/platform combinations will be referred to in a similar manner.

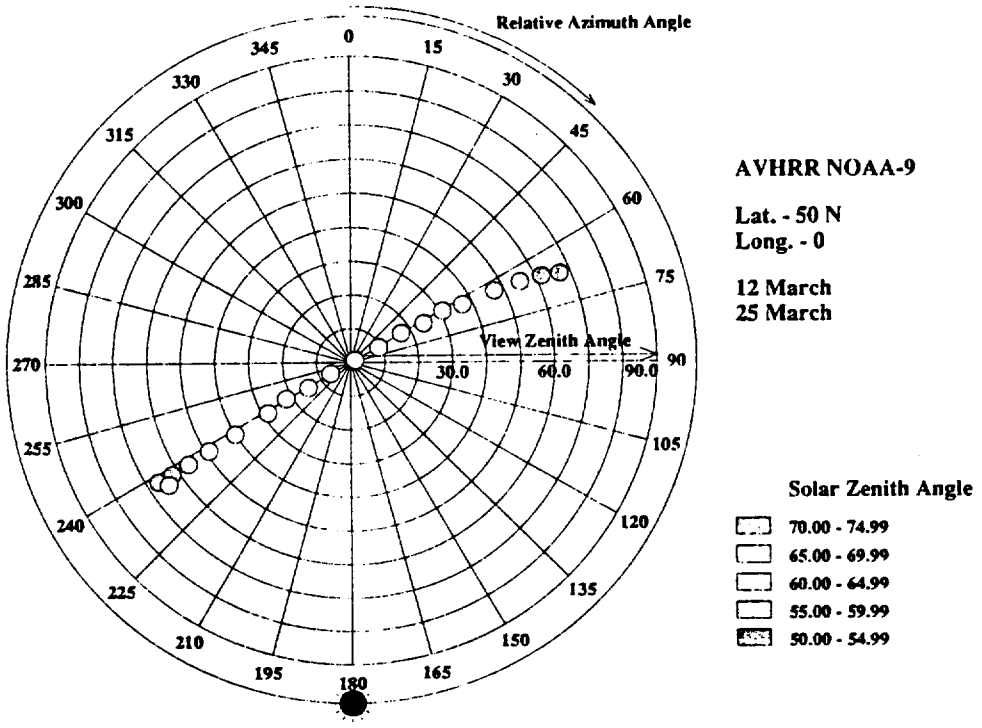

FIGURE 6 BRDF sampling capabilities of NOAA-9 AVHRR for a site at 50°N over a 16-day period around the March equinox. Concentric rings denote 10° increments of view zenith angle (θ_r), ranging from 0° (i.e. nadir) at the center of the plot to 90° at the edge. Radial lines denote 15° increments of *relative* azimuth angle (ψ), where 0° is the forescatter direction and 180° is the backscatter direction. N.B. The dots have been enlarged for diagrammatic purposes. (See color plate I at the back of the journal.)

angles center around 95°/285° depending on whether the orbital track is to the east or the west of the ground point. Solar zenith angles range from 52° to 71°, while the solar azimuth angles center on 217° and range from 201° to 245°.

Although Table 3 provides a complete description of the viewing and illumination geometry, it is tedious to work with. Instead, we have developed a graphical display that carries the same information (Figure 6). In this polar plot, the position of each 'dot' symbol indicates the viewing geometry at which a given point on the ground is observed from one of a series of orbital overpasses of the satellite sensor. As in Figures 3–5, the view zenith angle is plotted radially outwards from the center (nadir). However, the angular position of each 'dot' around the plot now indicates the *relative* azimuth angle between the sun and the sensor (ψ; where, by convention $\psi = |\phi_r - \phi_i| + 180°$). Thus $\psi = 180°$ denotes data collected in the backscatter direction. Finally, there remains the display of the solar zenith angle, which is indicated by the shading pattern of each dot symbol. The finished plot clearly indicates the capability of the sensor to sample the BRDF of the target. For example, from Figure 6 we would conclude that NOAA-9 AVHRR samples the viewing hemisphere—at this location and point in time—in a 'slice' about 60° from the solar principal plane ($\psi = 0°/180°$). Using this sensor, under

these conditions, important information contained in the BRDF around the hot spot cannot therefore be determined.

It is not our intention here to provide an exhaustive review of the angular sampling capabilities of all possible satellite sensors. Instead, we concentrate on four current instruments (Landsat TM, SPOT-HRV, NOAA-AVHRR and ERS-1 ATSR) and two sensors scheduled for launch in the near future as part of NASA's Earth Observing System (EOS) (MODIS-N and MISR). These illustrate the type of angular sampling that can be achieved using different configurations of sensor geometry and satellite orbital parameters. Despite its recent de-selection from the EOS programme, simulations are also performed for HIRIS, since this illustrates the BRDF sampling capabilities which may become available at some point in the future using an instrument that combines along-track and across-track pointing.

Current Satellite Sensors

Landsat TM

Since the Thematic Mapper's (TM) design precludes viewing points on the ground more than a few degrees from nadir, it cannot sample the BRDF well with respect to viewing angle. Despite this, it may still be possible to exploit changes in angular reflectance—as a function of the seasonal variation in solar zenith and solar azimuth angles—as a source of information. However, the ability to do even this is limited by the fixed (9:30am) equatorial crossing time of Landsat's orbit, which reduces the range of solar zenith angles encountered, except at very high latitudes. In any event, this strategy requires measurements assembled over a solstice-to-solstice period and is clearly only feasible over targets that might reasonably be expected to maintain their surface reflectance properties more or less unchanged during this period of time. Polar ice caps and deserts are possible candidates.

Table 4 provides a listing of TM looks and their geometry for a site at latitude 16°N, equivalent to the southern Sahara, for the period between the June and December solstices. A polar plot (Figure 7) of these data shows that the view angles are always close to nadir. Moreover, the solar zenith angle only varies between 30° and 50°. Given this limited sampling capability and the long time periods required for data acquisition, it seems appropriate to conclude that TM is unlikely to be a useful tool for BRDF studies; although this is not to say that measured reflectances in TM data are unaffected by the BRDF of earth surface materials.

SPOT-HRV

SPOT's across-track pointing capability effectively extends its scan angle to ±31.13° (i.e. 27° plus half the FOV, 4.13°), which yields a range of view zenith angles of ±35.8° at the ground. However, since the HRV sensors are fixed in the along-track direction they can only acquire data for a single 'slice' through the viewing hemisphere. Figure 8 presents polar plots for the SPOT-HRV sensors

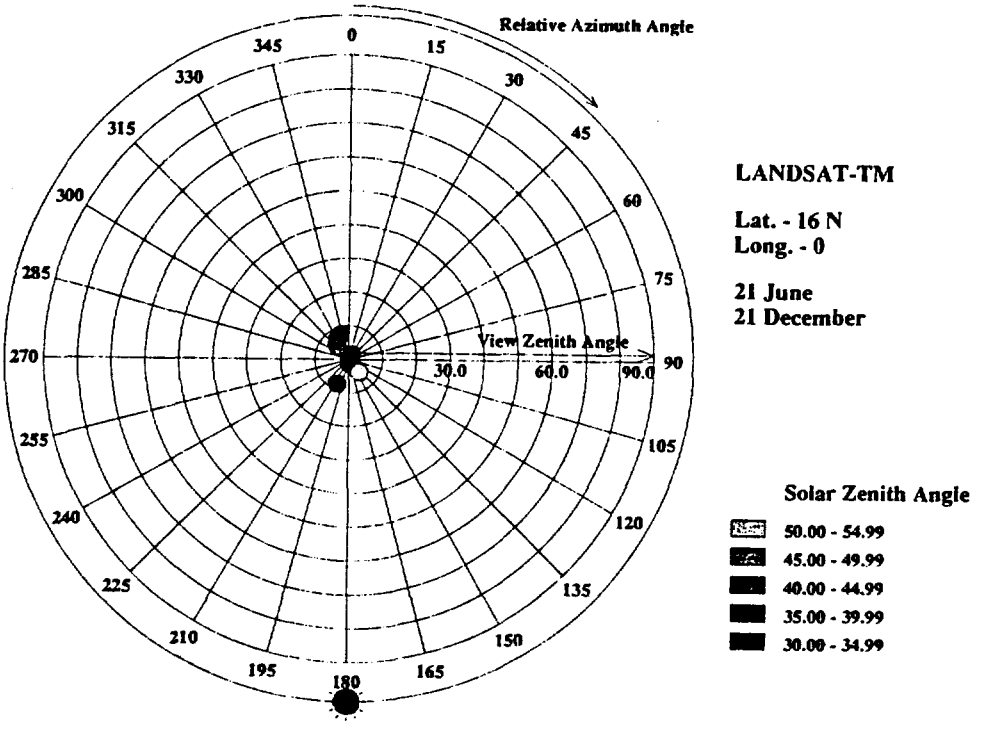

FIGURE 7 BRDF sampling capabilities of Landsat-TM for a site at 50°N over the period between the June and December solstices. Concentric rings denote 10° increments of view zenith angle (θ_r), ranging from 0° (i.e. nadir) at the center of the plot to 90° at the edge. Radial lines denote 15° increments of *relative* azimuth angle (ψ), where 0° is the forescatter direction and 180° is the backscatter direction. N.B. The dots have been enlarged for diagrammatic purposes. (See color plate II at the back of the journal.)

TABLE 4
Viewing and Illumination Geometry for Images Acquired for a Ground Point at 16°N by Landsat TM (10.00 Local Solar Time) Between the June and December Solstices

Julian Day	View Zenith Angle (°)	View Azimuth Angle (°)	Solar Zenith Angle (°)	Solar Azimuth Angle (°)	Relative Azimuth Angle (°)
177	1.9	279.1	49.1	37.5	61.6
202	0.9	279.9	47.0	40.1	59.8
227	0.0	0.0	42.3	46.7	0.0
252	1.1	97.5	36.5	57.9	219.5
277	2.1	98.0	31.8	73.7	204.3
302	3.1	98.3	29.5	90.9	187.4
318	6.3	278.5	28.4	100.1	358.5
327	4.0	99.3	29.4	104.0	174.4
343	5.3	278.6	28.8	108.6	350.0
352	5.0	98.4	29.8	109.2	169.2

for sites at latitude 50°N and the equator over 16-day periods around the March equinox and June solstice. Due to the changing position of the sun and the nature of SPOT's orbital track, the BRDF sampling pattern rotates clockwise both with changing latitude, from north to south (Figures 8a and 8b), and with the time of year, from the March equinox and the June solstice (Figures 8c and 8d). This rotation will occur in the angular sampling pattern of any instrument in a similar orbit. Figure 8b demonstrates that at certain times of the year and at certain latitudes the SPOT-HRV sensors may be able to acquire data in the solar principal plane and, more importantly, close to the hot spot. However, in the example shown the solar zenith angle is very small. As a result, angular reflectance effects are likely to be limited, due to the lack of shadows cast by vertical scene elements (e.g. leaves, trees, terrain facets) (Suits, 1972; Kimes, 1983; Li and Strahler, 1992).

NOAA-AVHRR

Although the AVHRR sensors on the NOAA-series of satellites do not possess the off-nadir pointing capability of the SPOT-HRV instruments, their very wide cross-track field-of-view (110°) enables data to be collected at view zenith angles up to ±70° (taking into account the effect of earth surface curvature). As a consequence of this, there is a considerable degree of overlap between images collected from adjacent orbital tracks—especially at high latitudes—such that a fixed point on the ground can be viewed at a number of different angles during the orbital repeat cycle. Moreover, AVHRR sensors can be used to acquire data for up to three different 'slices' through the viewing hemisphere. This is possible by virtue of the fact that almost identical devices are currently operating on a series of satellites with the same nominal orbital parameters, but with different equatorial crossing times (e.g. 7:30am and 7:30pm for NOAA-10; 2:00am and 2:00pm for NOAA-9 and 11[8]). This means that the angular reflectance properties of the earth surface can usually be measured on several occasions in a single day. The BRDF of a given point on the ground can therefore be sampled over a much wider range of solar zenith and solar azimuth angles than is possible using SPOT-HRV.

Figures 6 and 9 illustrate the BRDF sampling capabilities for AVHRR sensors on board NOAA-9 and NOAA-10, respectively. Data acquired during NOAA-10's early morning overpass are of particular interest, since they are sampled close to the solar principal plane and at large solar zenith angles (Figure 9). Using this sensor/platform combination, it may be possible to derive information on surface biophysical parameters contained within the BRDF at and around the hot spot, provided that atmospheric effects can be accounted for.

ERS-1 ATSR

The Along-Track Scanning Radiometer (ATSR) on board ERS-1 is unusual among current sensors in that it is capable of acquiring angular reflectance data

[8]The 2:00am (i.e. night-time) orbital overpass of NOAA-9 and 11 is clearly not relevant in this context.

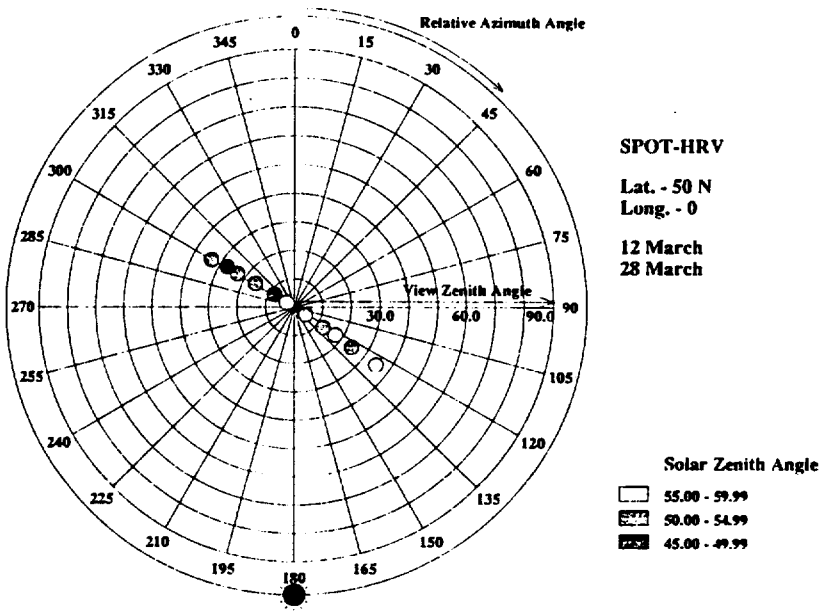

(a)

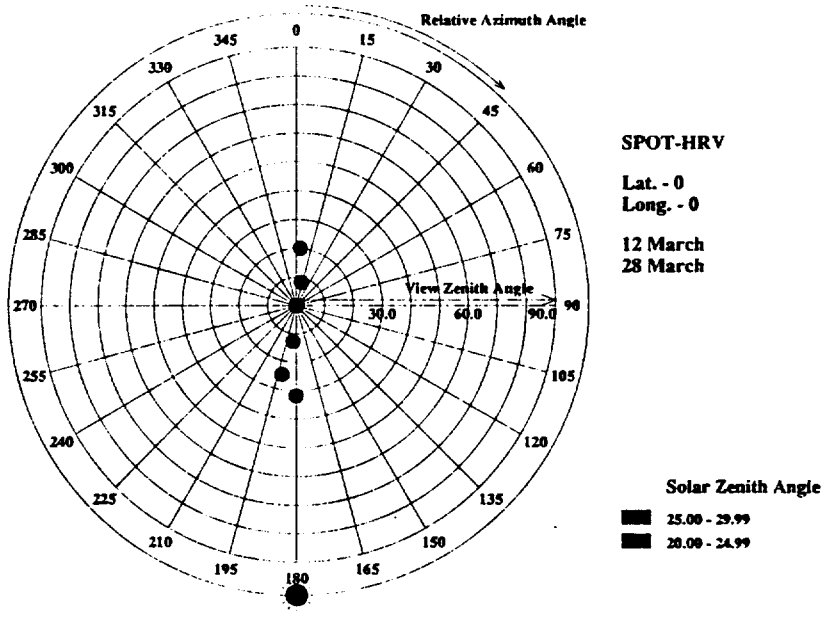

(b)

FIGURE 8 BRDF sampling capabilities of SPOT-1 HRV. (a) For a site at 50°N over a 16-day period around the March equinox. (b) For a site at 0°N over a 16-day period around the March equinox. (c) For a site at 50°N over a 16-day period around the June solstice. (d) For a site at 0°N over a 16-day period around the June solstice. Concentric rings denote 10° increments of view zenith angle (θ_r), ranging from 0° (i.e. nadir) at the center of the plot to 90° at the edge. Radial lines denote 15° increments of *relative* azimuth angle (ψ), where 0° is the forescatter direction and 180° is the backscatter direction. N.B. The dots have been enlarged for diagrammatic purposes. (See color plates III and IV at the back of the journal.)

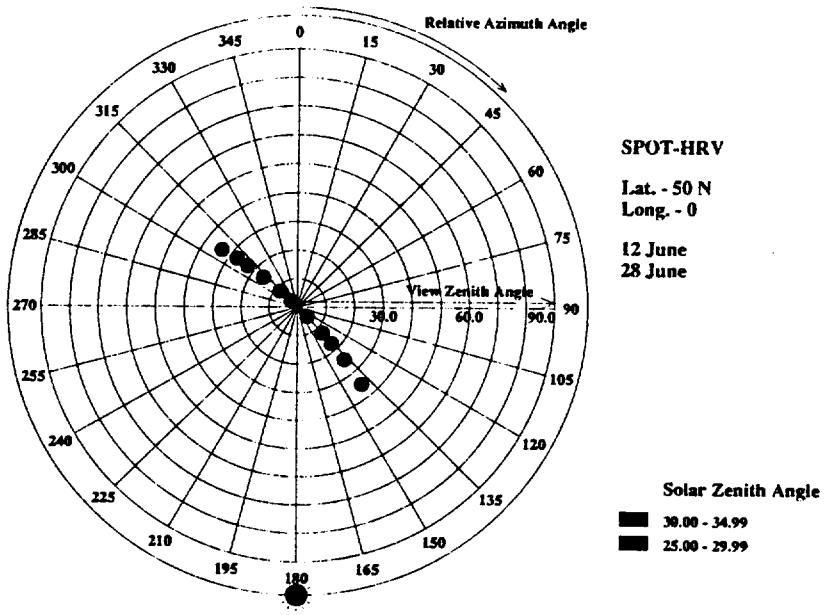

(c)

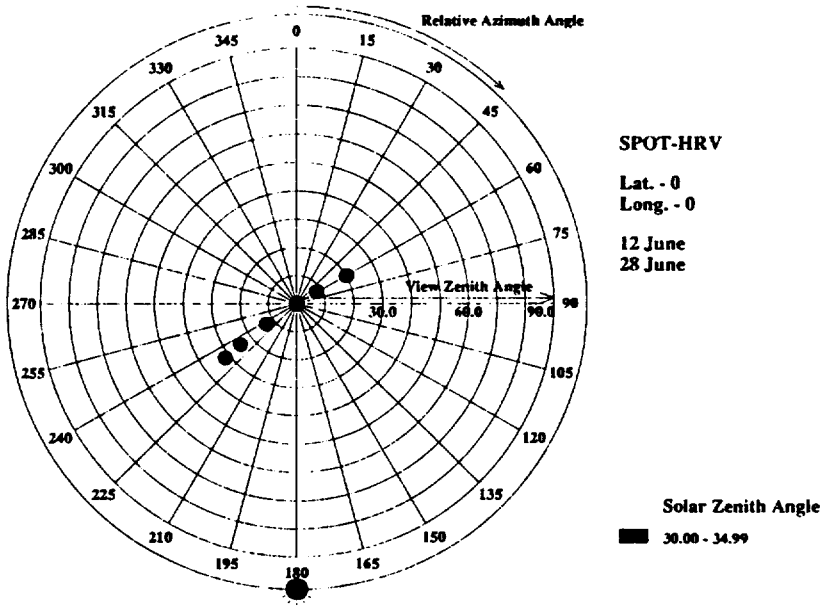

(d)

FIGURE 8 (*Continued*).

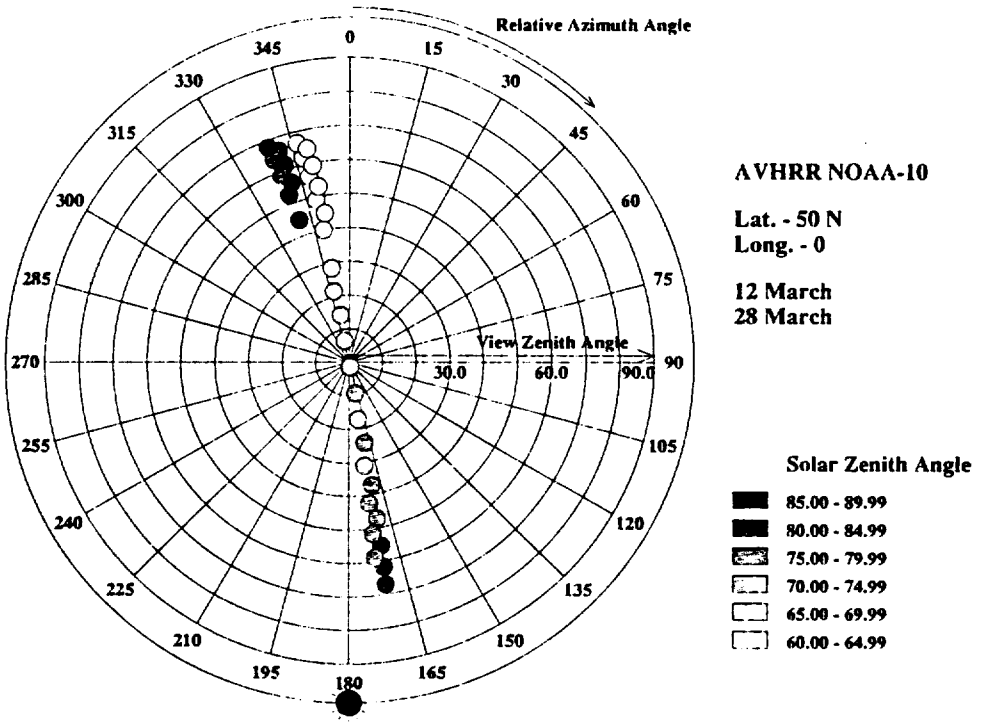

FIGURE 9 BRDF sampling capabilities of NOAA-10 AVHRR for a site at 50°N over a 16-day period around the March equinox. Concentric rings denote 10° increments of view zenith angle (θ_r), ranging from 0° (i.e. nadir) at the center of the plot to 90° at the edge. Radial lines denote 15° increments of *relative* azimuth angle (ψ), where 0° is the forescatter direction and 180° is the backscatter direction. N.B. The dots have been enlarged for diagrammatic purposes. (See color plate V at the back of the journal.)

at two view angles within a single orbital overpass. This is achieved by virtue of its novel conical scanning pattern, so that data are acquired along two arcs—the first centered on the sub-satellite point (i.e. nadir-looking), the second pointed forward of the satellite at 46.9° in the along-track direction (equivalent to a view zenith angle of 55°). Since the across-track field-of-view of ATSR-1 is 102°, multiple measurements of directional reflectance can also be obtained for a fixed ground point using overlapping images acquired from adjacent orbital paths.

Figure 10 illustrates the BRDF sampling pattern that can be achieved using ATSR-1 over a 16-day period around the March equinox, for a site at latitude 50°N. Data acquired on the nadir-viewing and forward pointing sections of the conical scan can be clearly identified, forming separate 'slices' across the viewing hemisphere. The distribution of the angular reflectance measurements is such that only one quadrant of the viewing hemisphere is sampled. This sampling pattern may, under certain circumstances, be adequate to provide a simple empirical description of the surface BRDF for, say, the correction of angular reflectance effects in images acquired by other orbital sensors or for albedo estimation. However, important information on reflectance variation around the hot spot is unavailable. Consequently, the use of such data to invert the BRDF, to infer values of key biophysical parameters, is likely to be limited.

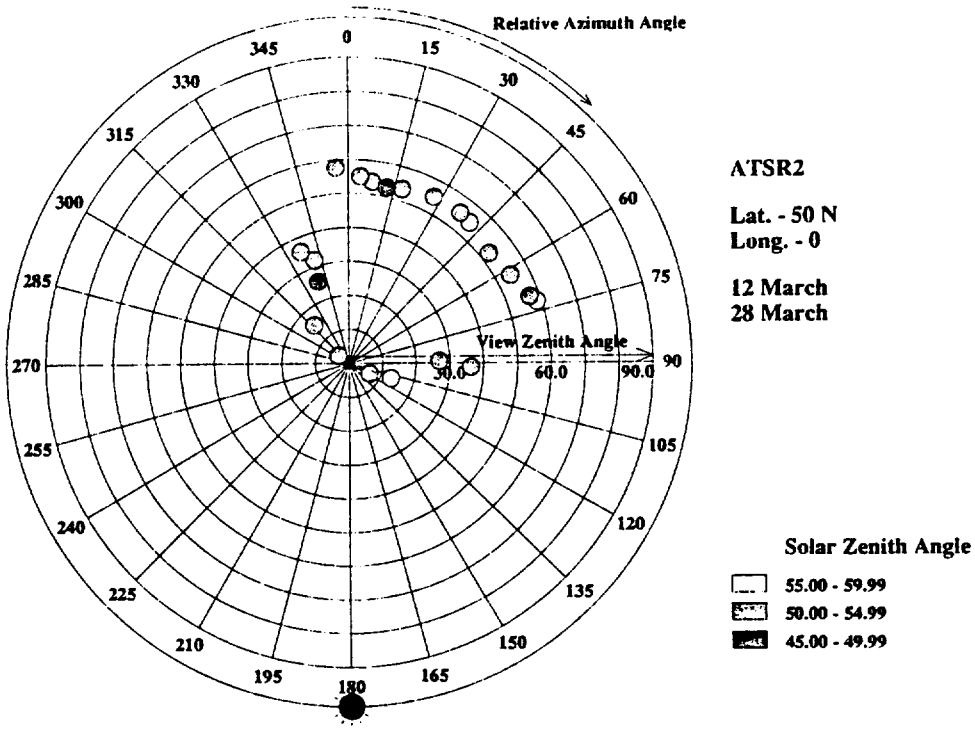

FIGURE 10 BRDF sampling capabilities of ERS-1 ATSR for a site at 50°N over a 16-day period around the March equinox. Concentric rings denote 10° increments of view zenith angle (θ_r), ranging from 0° (i.e. nadir) at the center of the plot to 90° at the edge. Radial lines denote 15° increments of *relative* azimuth angle (ψ), where 0° is the forescatter direction and 180° is the backscatter direction. N.B. The dots have been enlarged for diagrammatic purposes. (See color plate VI at the back of the journal.)

Future Satellite Sensors

MODIS-N

As one of the key instruments of NASA's proposed Earth Observing System, MODIS-N will fly on both the morning (EOS-AM) and afternoon (EOS-PM) overpass platforms (NASA, 1990). MODIS-N is designed to provide comprehensive and frequent global coverage in 36 spectral wavebands and at several different spatial resolutions (nominally 250 m, 500 m and 1 km dependent on the waveband). Ambitious studies of the land, oceans and atmosphere are planned for this instrument.

In many respects, the viewing geometry of MODIS-N will be similar to that of the current generation of NOAA-AVHRR devices. Specifically, MODIS-N will have a 110° across-track field-of-view (i.e. ±55°). Consequently, like NOAA-AVHRR, MODIS-N will be capable of acquiring multiple measurements of angular reflectance for a fixed field site by virtue of the high degree of overlap between images obtained on separate orbital overpasses.

Figure 11a illustrates the BRDF sampling capabilities of MODIS-N on the EOS-PM platform for a site at 50°N. The resemblance between the sampling

pattern for this sensor and that of the NOAA-9 AVHRR (Figure 6), which has a similar equatorial crossing time and orbital inclination angle, can be clearly seen. Both sensors record data in a single 'slice' across the BRDF oriented at roughly 60° with respect to the solar principal plane. The main difference between the two BRDF sampling patterns relates to the solar zenith angle at the time of imaging. As a result of its slightly earlier equatorial crossing time (13.30, compared with 14.30 for NOAA-9), MODIS-N will sample angular reflectance measurements at a somewhat smaller solar zenith angle than the AVHRR currently mounted on board NOAA-9.

Figure 11b shows the angular sampling pattern that will be possible using MODIS-N mounted on the EOS-AM platform. Once again, data will be recorded in a single 'slice' across the viewing hemisphere. The 'slice' will, however, be rotated with respect to that sampled by MODIS-N on the EOS-PM platform. This is due to the difference in their proposed equatorial crossing time and direction (10.30 descending node for EOS-AM, and 13.30 ascending node for EOS-PM) and, hence, in the relative azimuth angle at the time of imaging. Interestingly, though, the range of solar zenith angles over which data will be sampled is approximately the same for both the EOS-AM and EOS-PM instruments. This will mean that, all other things being equal, data from the two sensors could be merged together in a relatively straightforward manner. This type of data set would be suitable for use even with a comparatively simple empirical model of surface scattering, such as that developed by Walthall et al. (1985), to estimate the hemispherical reflectance and albedo of the observed surface.

MISR

Also proposed for inclusion on the EOS-AM platform is the MISR instrument. MISR will consist of nine CCD-array cameras recording image data simultaneously at nadir and at four off-nadir angles between 23.3° and 58.0° (equivalent to view zenith angles of 26.1° and 70.5°, respectively) along-track in both the fore and aft directions. Since all of the cameras will operate simultaneously, nine separate views of a target can be obtained during any one overpass. However, despite the fact that MISR's range of look angles is very large in the along-track direction, its field-of-view is relatively narrow in the across-track direction (28° for the nadir-viewing camera), providing a 356 km-wide swath.

Figure 12 demonstrates MISR's BRDF sampling capabilities for a site at 50°N, around the March equinox. This illustrates that MISR samples angular reflectance data within a narrow strip across the viewing hemisphere, with the strip tapering towards large view zenith angles. The latter effect is due to the different focal lengths used for each of the CCD cameras, designed to maintain a constant spatial resolution at the center of each of the corresponding scan lines. Thus, the cross-track field-of-view of the CCD cameras varies inversely with sensor look angle. For the latitude and time of year shown in Figure 12, MISR samples the BRDF around the 30°/210° relative azimuth plane. Since most natural surfaces display greatest variation in angular reflectance in the solar principal plane (i.e. $\psi = 0°/180°$), data collected by MISR under these

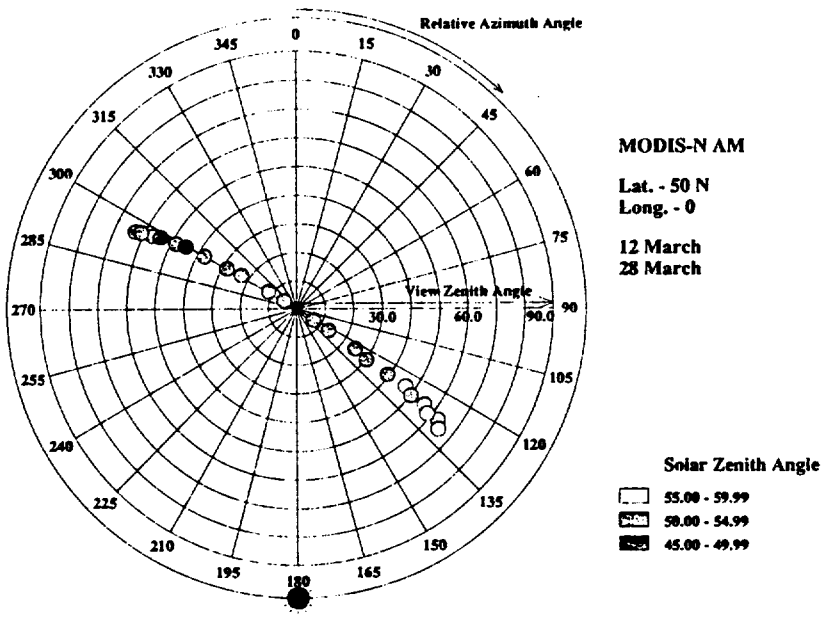

(a)

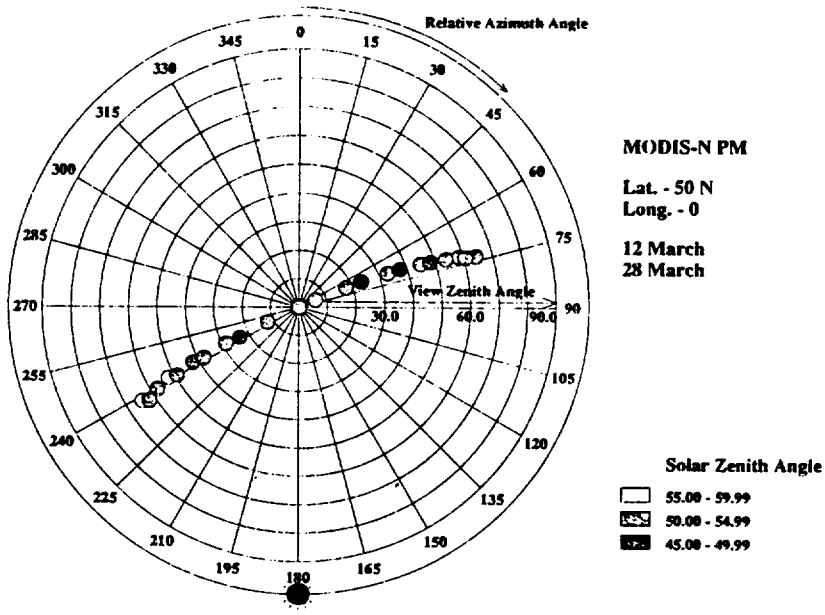

(b)

FIGURE 11 BRDF sampling capabilities of MODIS-N for a site at 50°N over a 16-day period around the March equinox. Concentric rings denote 10° increments of view zenith angle (θ_r), ranging from 0° (i.e. nadir) at the center of the plot to 90° at the edge. Radial lines denote 15° increments of *relative* azimuth angle (ψ), where 0° is the forescatter direction and 180° is the backscatter direction. N.B. The dots have been enlarged for diagrammatic purposes. (a) EOS-AM; (b) EOS-PM. (See color plate VII at the back of the journal.)

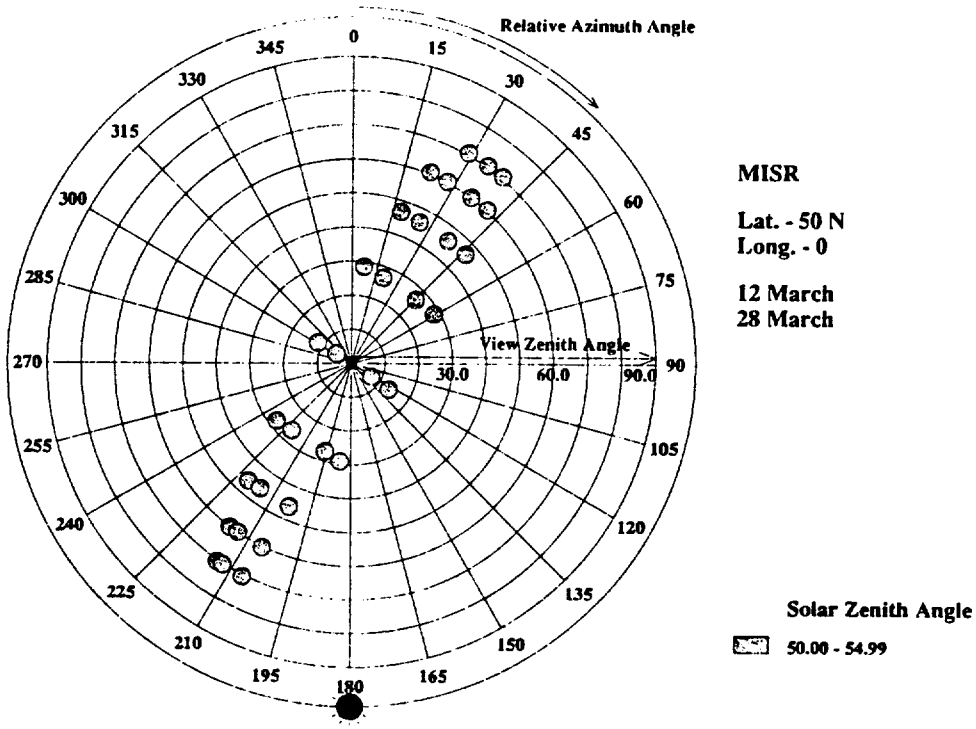

FIGURE 12 BRDF sampling capabilities of MISR on EOS-AM for a site at 50°N over a 16-day period around the March equinox. Concentric rings denote 10° increments of view zenith angle (θ_r), ranging from 0° (i.e. nadir) at the center of the plot to 90° at the edge. Radial lines denote 15° increments of *relative* azimuth angle (ψ), where 0° is the forescatter direction and 180° is the backscatter direction. N.B. The dots have been enlarged for diagrammatic purposes. (See color plate VIII at the back of the journal.)

conditions might be expected to provide a reasonably accurate estimate of the *degree* of reflectance anisotropy exhibited by the surface under observation.

Although MISR provides a relatively dense sample of the BRDF within the observable strip, the remainder of the viewing hemisphere remains un-sampled. Consequently, information on the *form* of the BRDF in these regions is unavailable. This situation is not unique to MISR—MODIS-N shares this characteristic. However, as was demonstrated earlier (Section 4.2.1), with MODIS-N it will be possible to combine data from identical instruments on board the EOS-AM and EOS-PM platforms to sample in two 'slices' across the viewing hemisphere, almost orthogonal to one another (Figure 11). As a result, the observations of angular reflectance are distributed more widely across the viewing hemisphere than is possible using MISR; although MISR samples closer to the solar principal plane and, hence, the hot spot. In an operational situation, it may be necessary to combine angular reflectance data from MISR with that recorded by other off-nadir viewing sensors, such as MODIS-N, to provide a sufficiently comprehensive angular sample of the complete BRDF. Availability of identical MISR instruments on both EOS-AM and EOS-PM would, of course, serve the same purpose.

HIRIS

Although HIRIS is no longer scheduled for launch as part of NASA's EOS programme, it is instructive to examine the BRDF sampling capability that it would have provided, as an example of what could be achieved using an instrument that can be pointed in both the along-track and across-track directions.

Unlike most EOS sensors, HIRIS was intended to provide high spatial resolution (30 m) images in 192 narrow spectral wavebands. To achieve this, while keeping data rates down, the design specifications for HIRIS utilised a relatively narrow field-of-view (2.1°), producing a swath of approximately 30 km on the ground. To compensate for this, and to allow examination of the angular reflectance properties of earth surface materials, HIRIS was intended to have the capability to be pointed off-nadir in both the along-track (56° to −30°, fore to aft) and across-track (±45°) directions.

Since HIRIS was not intended to provide comprehensive coverage of the earth surface on a regular basis, it is possible to consider its use in novel ways for BRDF sampling. For instance, if HIRIS were dedicated to the collection of angular reflectance data, it would be possible to tilt the instrument such that it could acquire multiple images for a small test site as the satellite approached the target, flew directly overhead, and then receded from it. This might be termed 'stare' mode. More interestingly still, HIRIS could be operated in 'stare' mode, not only when the sub-satellite track passed directly through the test site, but also on adjacent orbital overpasses, taking advantage of the sensor's cross-track pointing capability. In this way, data could be acquired for the test site over a wide range of view zenith and view azimuth angles, within a comparatively short period of time.

Figure 13 demonstrates the BRDF sampling that would be possible by operating an instrument such as HIRIS in 'stare mode' during a single orbital repeat cycle around the March equinox, for a test site at 50°N. The simulation assumes that the sensor is mounted on board a satellite with nominal orbital parameters similar to that of EOS-PM. As with all of the previous figures, it also assumes the complete absence of cloud cover during the period of observation. Figure 13 demonstrates the capability of an instrument such as HIRIS to sample angular reflectance data from within a large section of the viewing hemisphere. Indeed, apart from the very extreme view zenith angles, the only part of the BRDF that remains un-sampled is in the forward-scatter direction. This is partially compensated for by the fact that the BRDF is sampled particularly densely in the backscatter direction, including the hot spot, thereby opening up opportunities to study both the *magnitude* and the *shape* of this feature. With the aid of a suitable physical model of surface scattering, it would therefore be possible to use data acquired by an instrument such as HIRIS to infer fundamental biophysical parameters describing the reflecting surface.

DISCUSSION

In the preceding sections discussion has focused almost exclusively on the geometric considerations involved in sampling surface BRDFs using various sen-

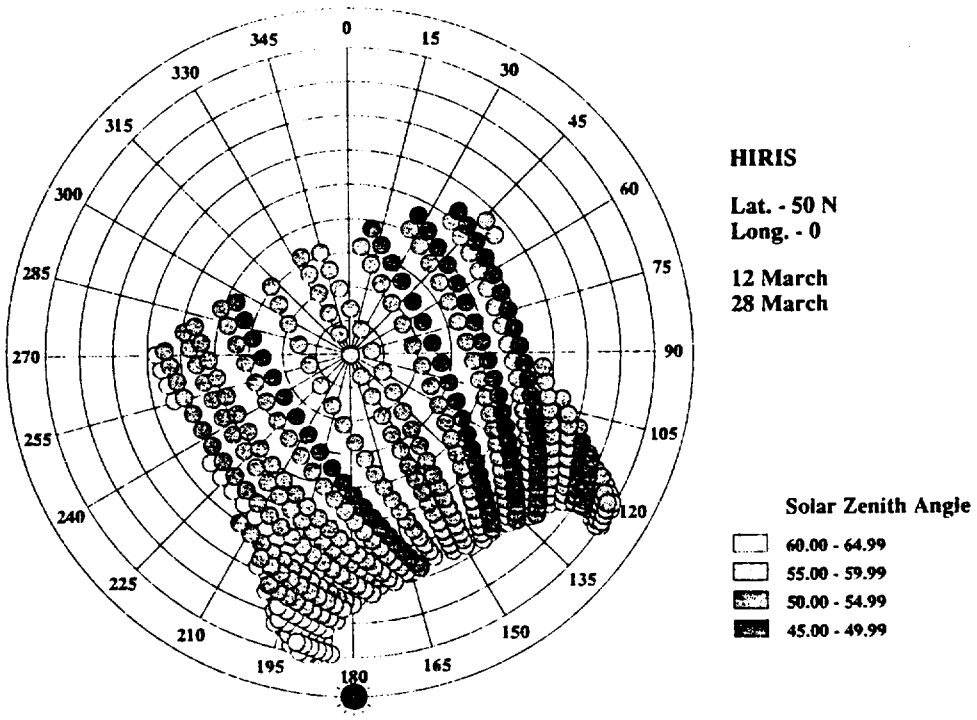

FIGURE 13 BRDF sampling capabilities of a HIRIS-type sensor mounted on board a satellite with the same nominal orbital parameters as EOS-AM for a site at 50°N over a 16-day period around the March equinox. Concentric rings denote 10° increments of view zenith angle (θ_r), ranging from 0° (i.e. nadir) at the centre of the plot to 90° at the edge. Radial lines denote 15° increments of *relative* azimuth angle (ψ), where 0° is the forescatter direction and 180° is the backscatter direction. N.B. The dots have been enlarged for diagrammatic purposes. (See color plate IX at the back of the journal.)

sor/platform combinations. Emphasis has been placed on factors such as the nominal maximum view angle(s) of the sensor and the equatorial crossing time of the satellite platform. While this is entirely valid and permits comparisons between different sensor/platform combinations, it does not address all aspects of determining surface BRDFs and inverting them to extract biophysical properties. In reality, a detailed consideration of a number of other points is also required. These include:

(i) the effect of spectral variability in the surface BRDF, especially when this is convolved with the spectral resolution of the sensor;
(ii) the relationship between the spatial resolution of the sensor and the dominant scale(s) of scene structure affecting the surface BRDF;
(iii) the requirement to derive information on surface bidirectional reflectance from exo-atmospheric measurements of radiance; and
(iv) the need to fit some function to the derived bidirectional reflectance data in order to extract the surface BRDF and, thus, to infer biophysical properties.

While it is not within the scope of this paper to cover all of these points in detail, this section attempts to outline some of the critical issues and to suggest ways in which they might be addressed.

Spectral Variability of Surface BRDFs

If the reflectance properties of a surface vary spectrally, then it is reasonable to expect that its BRDF will also be spectrally dependent. This may result from one of a number of reasons, including a change in the physical processes controlling the interaction of electromagnetic radiation with the surface at different wavelengths, and differential effects of multiple scattering within the surface layer. For example, in a vegetation canopy both the reflectance and the transmittance of leaves vary spectrally, especially in the visible and near-infrared wavelengths. At visible wavelengths, reflectance and transmittance are comparatively low, resulting in dark shadows cast by canopy elements. All other things being equal, this will result in a marked difference in the reflectance of the canopy measured at oblique sensor view angles pointing into and away from the sun (Kimes 1983). At near-infrared wavelengths, the reflectance and transmittance of the same leaves are much greater, resulting in less pronounced shadows. Moreover, since the target as a whole is brighter, multiple scattering within the canopy will tend to reduce the effect of shadows still further, suppressing the anisotropy of detected reflectance in the up-sun and down-sun directions (Kimes, 1983).

Inasmuch as all sensors that might be used to collect angular reflectance measurements are multispectral, it is instructive to consider how recovery of the BRDF and inference of surface biophysical parameters might be enhanced by using multispectral information. For the purpose of this discussion, we can consider the surface BRDF to be the product of two interacting sets of parameters—one set relating to the spectral characteristics of the surface materials, the other relating to their spatial and geometric arrangement. For a set of multispectral, multi-angle data acquired simultaneously by an imaging sensor, the geometric parameters may be considered to be constant (i.e. they are common to all images), whereas the spectrally-dependent parameters will—by definition—vary from band-to-band. Attempts to infer the geometric parameters are often based on inversion of a mathematical model of surface scattering using multi-angle data acquired in a single spectral waveband. However, if the spectral properties (e.g. reflectance, transmittance, phase function) of the canopy elements are known or can be generalised in advance, then a constrained inversion procedure can be used in which the structural parameters (e.g. leaf-angle distribution, leaf size, plant spacing) are selected as best fitting all multi-band measurements simultaneously. This approach has been used by Pinty et al. (1990) and Ross and Marshak (1989).

One issue arising from the use of multispectral, multi-angle data for model inversion is that of the minimum number of spectral wavebands and the optimum bandwidths required for this purpose. If the inversion procedure can be satisfactorily achieved using as few as four spectral wavebands, then MISR may prove to be a more than adequate source of such data. If, on the other hand, more wave-

bands are needed to constrain the inversion procedure, data from sensors such as MODIS-N may be required.

Effect of Sensor Spatial Resolution

It has already been noted that the current and future instruments capable of sampling surface BRDFs record data at very different spatial resolutions—nominally ranging from 15 m (ASTER) to 7 km (POLDER). Collection of angular reflectance data over such a wide range of resolutions has several implications. The first concerns how the spatial resolution of the sensor influences the information on the 3-D geometry of the surface material that is contained within the suite of angular reflectance measurements. For example, consider the hot spot produced by the three-dimensional structure of a surface or surface layer. Theoretical BRDF models have been devised for soils and regolith (e.g. Hapke, 1981, 1984, 1986; Ciernewski, 1987, 1989), discrete-leaf vegetation cover (Goel, 1987; Strahler and Jupp, 1990; Verstraete et al., 1990; Jupp and Strahler, 1991), whole (tree) canopy vegetation cover (Li and Strahler, 1986, 1992) and topographic surfaces (Hugli and Frei, 1983). Each of these operates at a different spatial scale and each produces a hot spot that theory shows to be invariant with spatial resolution. However, many real scenes are likely to contain all of these features. Does this mean that the observed hot spot will reflect all these levels of structure simultaneously, as theory might predict? Or will the effect be controlled by the one or two factors that are dominant at the resolution of the imaging device, as we might presuppose? At this point, the answer is not clear.

A further, related aspect of spatial resolution is that of areal coverage. If the primary objective of the study is to fit a physical model to a dense sample of angular reflectance measurements for a small region, then an instrument similar to HIRIS would be the sensor of choice. By operating in 'stare' mode, fixed on a ground patch of perhaps 30 km by 30 km, a HIRIS-type sensor would be capable of accumulating several dozen looks at the target within a few minutes (i.e. during a single overpass). MISR is also suited to such local area studies when operated in its 240 m resolution ('local area') mode for selected 360 km × 300 km regions. However, MISR's real strength lies in providing regular coverage of angular reflectance data over the entire earth surface in its 'Global mode' (960 m over the land and 1.92 km over the land).

The effect of spatial resolution is important not only when considering the comparability of angular reflectance data collected by different sensors, but also when considering consistency within an angular reflectance data set acquired by a single sensor. The issue here is one of variation in the dimensions of the ground resolution element (GRE) at different off-nadir view angles. Since most sensors, whether tilting or scanning, have a constant angular instantaneous field-of-view (IFOV) their GRE (i.e. the projected area of the IFOV on the earth surface) will increase with increasing sensor view angle. This is particularly pronounced for spaceborne sensors because of the combined effect of the increased path length from the sensor to the ground at off-nadir angles, and of earth surface curvature.

Changes in the dimensions of the GRE at different sensor view angles will introduce a number of problems—some tractable, some less so—for the consistent analysis of multi-angle images. These problems include: (i) added complexity for the geometric registration of multi-angle images, (ii) smoothing and/or aliasing of different BRDFs from adjacent surfaces as a result of spatial averaging, and (iii) variations in the dominant ground parameters affecting the measured angular reflectance data. The second two issues pose the greatest problems. Although they may have less effect on the derivation of accurate values for earth surface albedo, they will complicate considerably the extraction of meaningful values for specific biophysical parameters. In this context, the constant spatial resolution of all nine of MISR's CCD cameras, at least in the along-track dimension, may prove to be a telling advantage.

Deriving Information on Surface BRDFs from Exo-Atmospheric Measurements of Radiance

The atmosphere greatly influences measurements of reflectance made by spaceborne sensors, both in conditioning the spectral and angular distribution of radiation impinging on the target, and in modifying the photon stream as it exits the surface in the direction of the sensor. This situation is properly described by radiative-transfer theory, in which the surface BRDF acts as a boundary condition. However, solution of the radiative-transfer equations for a coupled atmosphere-surface model is complex and hardly practical for routine mapping applications.

Instead, a simpler, 'bulk' correction method is likely to be employed, in which atmospheric attenuation is determined from multispectral measurements of dark targets and aerosol properties are inferred from a regional aerosol climatology. With this information, it should be possible to exercise a rapid calculation code, such as 5S (Tanré et al., 1990), to produce a look-up table relating ground reflectance in a particular waveband to radiance as observed over a range of view angles. However, the reflectance values that are obtained by interrogating the table will be bidirectional reflectance factors (BRFs), not estimates of the BRDF, since they will include the effects of both direct and diffuse illumination. Nevertheless, since these reflectance factors are equivalent to spectral angular measurements commonly obtained in the field, in which angular radiance is ratioed to the radiance of a Lambertian panel, they will be immediately useful to a number of users.

Fitting a Function to the Surface BRDF

As was noted earlier in this paper, we may wish to use angular reflectance measurements for two contrasting purposes: (i) to characterise the angular scattering properties of the surface in some empirical way; and (ii) to infer basic physical parameters that govern the behaviour of the surface, through inversion of a physically-based model of surface scattering.

Empirical Characterisation

To go from BRFs to a characterisation of the whole BRDF, given a relatively sparse angular sample of spectral reflectance measurements, will necessitate constraining the BRDF to follow a fairly simple form, such as that devised by Walthall et al. (1985). An inversion procedure will be required to estimate the parameters of the BRDF that, given the angular distribution of irradiance field, yield the observed BRF values. If the objective is not necessarily to retrieve the full BRDF—for example, in 'correcting' an off-nadir measurement to its equivalent at nadir, or in estimating surface albedo—then simpler procedures may possibly prevail. If a more accurate characterisation of the BRDF is required, then methods such as spherical harmonics might be used (Barnsley and Muller, 1991). However, as the number of parameters increase, a greater number of angular reflectance samples are required to drive the model. If this requires multi-date measurements, then a trade-off occurs between the number of data points included and the errors that might be introduced through imprecise atmospheric correction or changes in surface characteristics that occur with time. We plan to develop these ideas more fully in a second paper in this series.

Physical Modelling

For the case in which we wish to apply and invert a physical model of the surface BRDF to infer values of the parameters that describe the 3-D structure of that surface, one approach is to utilise the BRFs that have been produced by the atmospheric correction algorithm. This would be equivalent to fitting a physical BRDF model to ground reflectance measurements, which has been reported in the literature on several occasions (Goel and Thompson, 1985; Goel and Grier, 1986; Goel, 1987; Pinty et al., 1990, Verstraete et al., 1990).

Because bulk atmospheric correction procedures may not be sufficiently accurate, it may be necessary to apply a combined atmosphere-surface parameter extraction procedure using a coupled model. Although this adds to the number of parameters that need to be fitted, it will also add considerably to the degrees of freedom, provided that we can consider the atmosphere to be homogeneous at a broader scale than the surface. We can also look to multispectral information to aid the extraction of atmospheric parameters. In the same way that some physical properties of the surface vary with wavelength and others (geometric ones) generally remain constant, so some atmospheric properties are highly spectrally dependent (attenuation length, single-scattering albedo of particulates) while others are less so (phase function).

Thus, accurate operational algorithms for surface-parameter extraction will most likely attack a multi-pixel region of multispectral, angular measurements, and exploit spatial, spectral and angular scales of variability simultaneously. Further development of this approach is the subject of a later paper in this series.

CONCLUSIONS

This paper has begun to analyse the capabilities of various satellite sensors for sampling the BRDF of earth surface materials. In the early phases of NASA's

EOS programme, MISR will be the primary source of angular reflectance measurements. Its capabilities will provide much of the information needed for BRDF applications, as well as pointing the way to BRDF-extraction algorithms for tilting imagers in the future. For parts of the viewing hemisphere that are poorly sampled by MISR, it may be necessary to augment these data with measurements made by MODIS-N on both the EOS-AM and EOS-PM platforms.

Clearly, synergistic use of all instruments making angular reflectance measurements will ultimately be required to obtain maximum information on surface BRDFs. In the light of this, studies should also be made of the implications of the differing spectral and spatial resolutions of these sensors. In particular, there is a need to examine both the optimum wavebands and minimum number of spectral channels required to represent the BRDF of natural surfaces adequately (Barnsley and Morris, 1990). It is also important to understand the meaning of BRDFs determined by sensors with spatial resolutions varying from a few hundred meters to several kilometers, in terms of important ecological and/or climatological parameters. Relatively little work has been undertaken in either of these two areas. This situation must be rectified soon, if the maximum potential of the EOS instruments is to be realised as each comes on line.

ACKNOWLEDGMENTS

We would like to thank the Natural Environment Research Council for support through Research Grant numbers GR3/7020 and GR3/7902 to Dr. Barnsley and Prof. Muller. Prof. Strahler's collaboration was supported by NASA contracts NAS5-30917 and NAS5-31369. Thanks are also due to Philip Lewis (Department of Geography, UCL) for discussions on BRDF sampling, and to Paul Schooling (Department of Geography, UCL) for his help and advice with the spherical trigonometry. The authors are also deeply indebted to Dr. Dave Diner, Dr. Anne Kahle and Dr. Pierre Deschamps for providing information on the current technical specifications of MISR, ASTER and POLDER, respectively.

References

Ardanuy, A., Han, D. and Salamonson, V. V. (1991) The Moderate Resolution Imaging Spectrometer (MODIS) Science and Data System requirements. *IEEE Transactions on Geoscience and Remote Sensing* **29**: 75–88.

Barnsley, M. J. (1984) Effects of off-nadir view angles on the detected spectral response of vegetation canopies. *International Journal Remote Sensing* **5**: 715–728.

Barnsley, M. J. and Kay, S. A. W. (1990) The relationship between sensor geometry, vegetation-canopy geometry and image variance. *International Journal of Remote Sensing* **11** (**6**): 1075–1084.

Barnsley, M. J. and Morris, K. P. (1990) Analysis of ground-level directional radiance spectra. In: *Proceedings of the Annual Conference of the Remote Sensing Society, Remote Sensing and Global Change*, University College Swansea, September 19–21, 1990, (Remote Sensing Society: Nottingham): 175–185.

Barnsley, M. J. and Muller, J-P. (1991) Measurement, simulation and analysis of the directional reflectance properties of earth surface materials. In: *Proceedings of the 5th International Colloquium—Physical Measurements and Signatures in Remote Sensing*, Courchevel, France, January 14–18 (ESA SP-319, May 1991): 375–382.

Brakke, T. W. and Otterman, J. (1990) Canopy bidirectional reflectance dependence on leaf orientation. *International Journal of Remote Sensing* **11** (**6**): 1023–1032.

Cierniewski, J. (1987) A model for soil surface roughness influence on the spectral response of bare soils in the visible and near-infrared range. *Remote Sensing of Environment* **23**: 97–115.

Cierniewski, J. (1989) The influence of the viewing geometry of bare rough soil surfaces on their spectral response in the visible and near-infrared range. *Remote Sensing of Environment* **27**: 135–142.

Deering, D. W., Eck, T. F. and Otterman, J. (1989) Bidirectional reflectances of three soil surfaces and their characterisation through model inversion. In: *Proceedings of IGARSS'89* **2**: 670–673.

Deschamps, P. Y., Herman, M., Podaire, A., Leroy, M., Laporte, M. and Vermande, P. (1990) A spatial instrument for the observation of polarization and directionality of earth reflectances: POLDER. In: *Proceedings of IGARSS'90*, Washington, DC: 1769–1774.

Deuzé, J-L., Balois, J-Y., Devaux, C., Gonzalez, L., Herman, M., Lecomte, P. and Verwaerde, C. (1991) Aircraft simulations of the POLDER experiment: First results. In: *Proceedings of the 5th International Colloquium—Physical Measurements and Signatures in Remote Sensing*, Courcheval, France, January 14–18 (ESA SP-319, May 1991): 393–396.

Diner, D. J. and Martonchik, J. V. (1985) Atmospheric transmittance from spacecraft using multiple view angle imagery. *Applied Optics* **24**: 3503–3511.

Diner, D. J. (1988) *Geophysical and Climatological Research Using a Multi-angle Imaging SpectroRadiometer (MISR)*. Instrument Investigation Proposal to NASA, Eos Programme: p. 65.

Diner, D. J., Bruegge, C. J., Martonchik, J. V., Ackerman, T. P., Davies, R., Gerstl, S. A. W., Gordon, H. R., Sellers, P. J., Clark, J., Daniels, J. A., Danielson, E. D., Duval, V. G., Klaasen, K. P., Lilienthal, G. W., Nakamoto, D. I., Pagano, R. J. and Reilly, T. H. (1989) MISR: A multiangle imaging spectroradiometer for geophysical and climatological research from EOS. *IEEE Transactions on Geoscience and Remote Sensing* **27**: 200–214.

Dorman, J. L. and Sellers, P. J. (1989) A global climatology of albedo, roughness length and stomatal resistance for atmospheric General Circulation Models as represented by the Simple Biosphere Model (SiB). *Journal of Applied Meteorology* **28**: 833–855.

Gerstl, S. A. W. and Simmer, C. (1986) Radiation physics and modelling for non-Lambertian surfaces. *Remote Sensing of Environment* **20**: 1–29.

Gerstl, S. A. W. and Zardecki, A. (1985) Coupled atmosphere/canop: Model for remote sensing of plant reflectance features. *Applied Optics* **24**: 94–103.

Goel, N. S. (1987) Models of vegetation canopy reflectance and their use in the estimation of biophysical parameters from reflectance data. *Remote Sensing Reviews* **3**: 1–212.

Goel, N. S. and Grier, T. (1986) Estimation of canopy parameters for inhomogeneous vegetation canopies from reflectance data. II. Estimation of leaf area index and percentage of ground cover for row canopies. *International Journal of Remote Sensing* **7**: 1263–1286.

Goel, N. S. and Reynolds, N. E. (1989) Bidirectional canopy reflectance and its relationship to vegetation characteristics. *International Journal of Remote Sensing* **10**: 107–132.

Goel, N. S. and Thompson, R. L. (1985) Optimal solar/viewing geometry for an accurate estimation of leaf area index and leaf angle distribution from bidirectional canopy reflectance data. *International Journal of Remote Sensing* **6**: 1493–1515.

Goel, N. S., Rozehnal, I. and Thompson, R. L. (1991) Vegetation canopies and objects of arbitrary shapes: Computer generation and bidirectional reflectance calculations. In: *Proceedings of the 5th International Colloquim—Physical Measurements and Signatures in Remote Sensing*, Courchevel, France, January 14–18 (ESA SP-319, May 1991): 409–413.

Goetz, A. F. H. and Herring, M. (1989) The High Resolution Imaging Spectrometer (HIRIS) for EOS. *IEEE Transactions on Geoscience and Remote Sensing* **GE-27**: 136–144.

Goward, S. N., Markham, B., Dye, D. G., Dulaney, W. and Yang, J. (1991) Normalized Difference Vegetation Index measurements from the Advanced Very High Resolution Radiometer. *Remote Sensing of Environment* **35**: 257–277.

Gutman, G. G. (1991) Vegetation indices from AVHRR: An update and future prospects. *Remote Sensing of Environment* **35**: 121–136.

Hapke, B. (1981) Bidirectional reflectance spectroscopy. 1. Theory. *Journal of Geophysical Research* **86**: 3039–3054.

Hapke, B. (1984) Bidirectional reflectance spectroscopy. 3. Correction for macroscopic roughness. *Icarus* **59**: 41–59.

Hapke, B. (1986) Bidirectional reflectance spectroscopy. 4. The extinction coefficient and the opposition effect. *Icarus* **67**: 264–280.

Hapke, B. and Wells, E. (1981) Bidirectional reflectance spectroscopy. 2. Experiments and observations. *Journal of Geophysical Research* **86**: 3055–3060.

Holben, B. and Fraser, R. S. (1984) Red and near-infrared sensor response to off-nadir viewing. *International Journal of Remote Sensing* **5:** 145–160.

Hugli, H. and Frei, W. (1983) Understanding anisotropic reflectance in mountainous terrain. *Photogrammetric Engineering and Remote Sensing* **49:** 671–683.

Ioltukhovski, A. A. (1991) Multiangular approach to solution of atmosphere optics reverse problems. In: *Proceedings ot the 5th International Colloquium—Physical Measurements and Signatures in Remote Sensing*, Courchevel, France, January 14–18 (ESA SP-319, May 1991): 423–425.

Jackson, R. D., Teillet, P. M., Slater, P. N., Fedosejevs, G., Jasinski, M. F., Aase, J. K. and Moran, M. S. (1990) Bidirectional measurements of surface reflectance for view angle corrections of bolique imagery. *Remote Sensing of Environment* **32:** 189–202.

Jupp, D. L. B. J. and Strahler, A. H. (1991) A hotspot model for leaf canopies. *Remote Sensing of Environment* **38:** 193–210.

Kriebel, K. T. (1978) Measured spectral bidirectional reflection properties of four vegetated surfaces. *Applied Optics* **17 (2):** 253–258.

Kimes, D. S. (1983) Dynamics of directional reflectance factor distributions for vegetation canopies. *Applied Optics* **22:** 1364–1372.

Kimes, D. S. and Sellers, P. J. (1985) Inferring hemispherical reflectance of the earth's surface for global energy budgets from remotely-sensed nadir or directional radiance values. *Remote Sensing of Environment* **18:** 205.

Kimes, D. S., Sellers, P. J. and Diner, D. J. (1987) Extraction of spectral hemispherical reflectance (albedo) of surfaces from nadir and directional reflectance data. *International Journal of Remote Sensing* **8:** 1727–1746.

Li, X. and Strahler, A. H. (1986) Geometrical-optical bidirectional reflectance modelling of a conifer forest canopy. *IEEE Transactions on Geoscience and Remote Sensing* **GE-24:** 906–919.

Li, X. and Strahler, A. H. (1992) Geometric-optical bidirectional reflectance modelling of the discrete-crown vegetation canopy: Effect of crown shape and mutual shadowing. *IEEE Transactions on Geoscience and Remote Sensing* **30:** 276–292.

Liang, S. and Strahler, A. H. (1993) The computation of radiance for coupled atmosphere and canopy media using an improved Gauss–Seidel algorithm. *IEEE Transactions on Geoscience and Remote Sensing*, in press.

Martonchik, J. V. and Diner, D. J. (1992) Retrieval of aerosol and land surface optical properties from multi-angle satellite imagery. *IEEE Transactions on Geoscience and Remote Sensing* **30:** 223–230.

NASA (1986a) *MODIS—Moderate Resolution Imaging Spectrometer*: Instrument Panel Report, Volume IIb, NASA, Washington, DC, p. 59.

NASA (1986b) *HIRIS—High Resolution Imaging Spectrometer: Science Opportunities for the 1990's*. Instrument Panel Report, Volume IIc, NASA, Washington, DC, p. 74.

NASA (1990) *EOS Instrument Directory*. NASA, Washington, DC, p. 118.

Nicodemus, F. E., Richmond, J. C., Hsia, J. J., Ginsberg, I. W. and Limperis, T. (1977) *Geometrical Considerations and Nomenclature for Reflectance*. NBS Monograph 160, Institute for Basic Standards, Washington, DC.

Otterman, J. (1985) Bidirectional and hemispheric reflectivities of a bright soil plane and a sparse dark canopy. *International Journal of Remote Sensing* **6:** 897–902.

Otterman, J., Strebel, D. E. and Ranson, K. J. (1987) Inferring spectral reflectances of planet elements by simple inversion of bidirectional reflectance measurements. *Remote Sensing of Environment* **21:** 215–228.

Paltridge, G. W. and Mitchell, R. M. (1990) Atmospheric and view angle correction of vegetation indices and grassland fuel moisture content derived from NOAA/AVHRR. *Remote Sensing of Environment* **31:** 121–135.

Pinker, R. T., Ewing, J. A. and Gruber, A. (1986) Diurnal variation of planetary radiation budget parameters from geostationary satellites. *Journal of Climatology* **6:** 389–403.

Pinty, B. and Raymond, D. (1987) A method for the estimation of broadband directional surface albedo from a geostationary satellite. *Journal of Climate and Applied Meteorology* **26:** 1709–1722.

Pinty, B., Verstraete, M. M. and Dickinson, R. E. (1989) A physical model for predicting bidirectional reflectances over bare soil. *Remote Sensing of Environment* **27:** 273–288.

Pinty, B., Verstraete, M. M. and Dickinson, R. E. (1990) A physical model of the bidirectional reflectance of vegetation canopies. 2. Inversion and validation. *Journal of Geophysical Research* **95:** 11767–11775.

Pinty, B. and Verstraete, M. M. (1991) Bidirectional reflectance and surface albedo: Physical modelling and inversion. In: *Proceedings of the 5th International Colloquim—Physical Measurements and Signatures in Remote Sensing*, Courcheval, France, January 14–18 (ESA SP-391, May 1991): 383–386.

Prata, A. J., Cechet, R. P., Barton, I. J. and Llewellyn-Jones, D. T. (1990) The Along-Track Scanning Radiometer for ERS-1: Scan geometry and data simulation. *IEEE Transactions on Geoscience and Remote Sensing* **28:** 3–13.

Powers, B. J. and Gerstl, S. A. W. (1988) Modeling of atmospheric effects on the angular distribution of a backscatter peak. *IEEE Transactions on Geoscience and Remote Sensing* **28:** 649–659.

Roujean, J. L., Leroy, M., Deschamps, P. Y. and Podaire, A. (1990) A surface BRDF model to be used for the correction of directional effects in remote sensing multitemporal data sets. In: *Proceedings of IGARSS'90*, May 21–24, 1990, Washington, DC.

Ross, J. K. and Marshak, A. L. (1988) Calculation of canopy directional reflectance using the Monte Carlo Method. *Remote Sensing of Environment* **24:** 213–225.

Ross, J. K. and Marshak, A. L. (1989) Influence of leaf orientation and the specular component of leaf reflectance on the canopy bidirectional reflectance. *Remote Sensing of Environment* **24:** 213–225.

Running, S. W., Justice, C. J., Strahler, A. H., Salomonson, V., Hall, D., Huete, A., Kaufman, Y., Muller, J-P., Vanderbilt, V., Wan, Z. M., Teillet, P. and Carneggie, D. (1993) Terrestrial remote sensing science and algorithms planned for EOS/MODIS. *International Journal of Remote Sensing*, in preparation.

Salomonson, V. V. and Marlatt, W. E. (1971) Airborne measurements of reflected solar radiation. *Remote Sensing of Environment* **2:** 1–8.

Salomonson, V. V., Barnes, W. L., Maymon, P. W., Montgomery, H. E. and Ostrow, H. (1989) MODIS: Advanced facility instrument for studies of the earth as a system. *IEEE Transactions on Geoscience and Remote Sensing* **GE-27:** 145–153.

Saunders, R. W. (1990) The determination of broad-band surface albedo from AVHRR visible and near-infrared radiances. *International Journal of Remote Sensing* **11:** 49–67.

Strahler, A. H. and Jupp, D. L. B. (1990) Modeling bidirectional reflectance of forests and woodlands using Boolean models and geometric optics. *Remote Sensing of Environment* **34:** 153–166.

Suits, G. H. (1972) The calculation of the directional reflectance of a vegetation canopy. *Remote Sensing of Environment* **2:** 117–125.

Tanré, D., Herman, M. and Deschamps, P. Y. (1983) Influence of the atmosphere on space measurements of directional properties. *Applied Optics* **22** (**5**): 733–741.

Tanré, D. C., Deroo, C., Duhaut, P., Herman, M., Morcrette, J. J., Perbos, J. and Deschamps, P. Y. (1990) Description of a computer code to simulate the satellite signal in the solar spectrum: 5S code. *International Journal of Remote Sensing* **11:** 659–668.

Verstraete, M. M., Pinty, B. and Dickinson, R. E. (1990) A physical model of the bidirectional reflectance of vegetation canopies. 1. Theory. *Journal of Geophysical Research* **95:** 11755–11765.

Walthall, C. L., Norman, J. M., Welles, J. M., Campbell, G., and Blad, B. L. (1985) Simple equation to approximate the bidirectional reflectance from vegetative canopies and bare soil surfaces. *Applied Optics* **24:** 383–387.